

Copyright
by
Haifeng Zhao
2010

The Dissertation Committee for Haifeng Zhao
certifies that this is the approved version of the following dissertation:

Modeling and Computing based on Lattices

Committee:

Gregory J. Rodin, Supervisor

Mark E. Mear

K. Ravi-Chandar

Dmitrii E. Makarov

Desiderio Kovar

Modeling and Computing based on Lattices

by

Haifeng Zhao, B.E., M.S.

DISSERTATION

Presented to the Faculty of the Graduate School of

The University of Texas at Austin

in Partial Fulfillment

of the Requirements

for the Degree of

DOCTOR OF PHILOSOPHY

THE UNIVERSITY OF TEXAS AT AUSTIN

December 2010

Dedicated with love
to my family.

Acknowledgments

First and foremost, I extend deep gratitude to my adviser Dr. Gregory J. Rodin, whose invaluable guidance, infinite patience, and constant support made the dissertation process a truly rich and enjoyable learning experience. His brilliant insight and genuine commitment to my scientific training and personal growth is unparalleled.

I also wish to express sincere appreciation to my committee members, Dr. Mark E. Mear and Dr. K. Ravi-Chandar from the Department of Aerospace Engineering and Engineering Mechanics, Dr. Dmitrii E. Makarov from the Department of Chemistry and Biochemistry, and Dr. Desiderio Kovar from the Department of Mechanical Engineering. They provided me with knowledge, wisdom and perspective that ultimately enriched the entire research and study process. My heartfelt appreciation also goes to Dr. Nickolay V. Shestopalov, Dr. Wen-Yea Jang, Han Tran and Reza Soheilifard for helping me during my Ph.D. studies.

Furthermore, I would like to thank my parents and my wife. This dissertation is a direct reflection of their loving support.

Modeling and Computing based on Lattices

Publication No. _____

Haifeng Zhao, Ph.D.

The University of Texas at Austin, 2010

Supervisor: Gregory J. Rodin

This dissertation presents three studies addressing various modeling and computational aspects of lattice structures. The first study is concerned with characterization of the threshold behavior for very slow (subcritical) crack growth. First, it is shown that this behavior requires the presence of a healing mechanism. Then thermodynamic analysis of brittle fracture specimens near the threshold developed by Rice (1978) is extended to specimens undergoing microstructural changes. This extension gives rise to a generalization of the threshold concept that mirrors the way the resistance R -curve generalizes the fracture toughness. In the absence of experimental data, the resistance curve near the threshold is constructed using a lattice model that includes healing and rupture mechanisms. The second study is concerned with transmission of various boundary conditions through irregular lattices. The boundary conditions are parameterized using trigonometric Fourier series, and it is shown that,

under certain conditions, transmission through irregular lattices can be well approximated by that through classical continuum. It is determined that such transmission must involve the wavelength of at least 12 lattice spacings; for smaller wavelength classical continuum approximations become increasingly inaccurate. Also it is shown that this restriction is much more severe than that associated with identifying the minimum size for representative volume elements. The third study is concerned with extending the use of boundary algebraic equations to problems involving irregular rather than regular lattices. Such an extension would be indispensable for solving multiscale problems defined on irregular lattices, as boundary algebraic equations provide seamless bridging between discrete and continuum models. It is shown that, in contrast to regular lattices, boundary algebraic equations for irregular lattices require a statistical rather than deterministic treatment. Furthermore, boundary algebraic equations for irregular lattices contain certain terms that require the same amount of computational effort as the original problem.

Table of Contents

Acknowledgments	v
Abstract	vi
List of Figures	x
Chapter 1. Introduction	1
1.1 Literature Review	1
1.1.1 Physical Lattices	2
1.1.2 Models Based on Lattices	3
1.1.3 Solution Methods	6
1.2 Introduction of Anti-plane Elastostatic Lattices	9
1.3 Dissertation Structure	10
1.3.1 The Resistance Curve for Subcritical Cracks Near the Threshold	12
1.3.2 On Continuum Approximation of Irregular Lattices . . .	12
1.3.3 On Extension of Boundary Algebraic Equations to Irreg- ular Lattices	13
Chapter 2. The Resistance Curve for Subcritical Cracks Near the Threshold	15
2.1 Introduction	15
2.2 Analysis	18
2.3 Simulation Methodology	22
2.3.1 Specimen Description	22
2.3.2 Bond Rupture and Healing	24
2.3.3 Implementation Details	26
2.4 Simulation Results	30
2.4.1 Crack Growth Versus Damage Accumulation	30

2.4.2	Quasi-brittle Regime	31
2.4.3	T -curve	33
2.5	Closure	37
Chapter 3.	On Continuum Approximation of Irregular Lattices	39
3.1	Introduction	39
3.2	Problem Formulation	41
3.3	Singular Value Decomposition	44
3.4	Simulation Results	48
3.5	Closing Remarks	54
Chapter 4.	On Extension of Boundary Algebraic Equations to Irregular Lattices	59
4.1	Introduction	59
4.2	Lattices	60
4.3	Green's Function	63
4.4	Boundary Algebraic Equation	63
4.5	Summary	66
Chapter 5.	Concluding Remarks	67
	Bibliography	69
	Vita	86

List of Figures

1.1	Representations of materials containing lattice structures: (a) Aluminum open-cell foam [55] ; (b) Cellular material [49] ; (c) Truss-like material [29] ; (d) Atomic network [103].	4
1.2	Examples of lattices: (a) Square lattice; (b) Delaunay lattice.	11
2.1	Clamped Mode I fracture specimen.	23
2.2	The fracture specimen for $M = 12$ (left); The crack tip and the coordinate system (right).	23
2.3	Rupture patterns for $\alpha = 100$ and $M = 12$: (a) Damage accumulation for $G = 1.02G_B$; (b) Damage and crack growth for $G = 7.97G_B$; (c) Curvilinear crack growth path for $G = 15.3G_B$; (d) Straight crack growth path for $G = 40.0G_B$	32
2.4	The T -curve for $\alpha = 100$ using specimens with $M = 8$ and $M = 12$	35
3.1	Circular lattice Ω (circle of radius R) and its subdomains: Domain of interest ω (circle of radius r); Deterministic buffer zone (ring with radii r and $\rho = r + \delta$); Statistical buffer zone (ring with radii ρ and R).	45
3.2	Error e_{v_i} verses the mode number i for (a) $\rho = 25, \delta = 5, \Delta = 5$; (b) $\rho = 25, \delta = 5, \Delta = 15$; (c) $\rho = 25, \delta = 5, \Delta = 25$	51
3.3	Discrete (symbols) versus continuum (lines) modes for $\rho = 25, \delta = 5, \Delta = 20$: (a) mode number 2 ($e_{v_2} = 0.11$), (b) mode number 12 ($e_{v_{12}} = 0.14$), (c) mode number 22 ($e_{v_{22}} = 0.27$), (d) mode number 32 ($e_{v_{32}} = 1.30$), (e) mode number 42 ($e_{v_{42}} = 1.34$). The threshold for $\epsilon = 0.3$ is $i_0 = 23$ and the wave number $k_0 = 11$	52
3.4	Error e_{v_i} verses the mode number i for (a) $\rho = 20, \delta = 2, \Delta = 20$; (b) $\rho = 20, \delta = 5, \Delta = 20$; (c) $\rho = 20, \delta = 10, \Delta = 20$	53
3.5	The threshold wavelength λ_0 versus ρ	55
3.6	The coefficient of variation for the overall shear modulus versus the RVE diameter.	57

4.1	(a) Quasi-spherical domain Ω ; (b) Quasi-spherical shell Ω^+ ; (c) The interface between Ω^- and Ω^+ involving the nodes $\partial\Omega^-$ (solid circles) and Γ^i (unfilled circles), and the bonds Ω^0	62
-----	---	----

Chapter 1

Introduction

This dissertation consists of three modeling and computing studies based on lattices. The first study is concerned with a threshold resistance T -curve for subcritical cracks based on the competition between rupture and healing. The second study is concerned with establishing new relationships between true discrete and approximate continuum descriptions of irregular lattices. The third study is concerned with the applicability of boundary algebraic equations for multiscale modeling of irregular lattices.

In the following section, we will give a general account of the background and literature review associated with lattices. The next three chapters will consist of their own literature reviews concerning each of the studies covered in this dissertation.

1.1 Literature Review

The beauty of the lattice models is in their simplicity. Here, we are mainly concerned with applications of lattice models in the mechanics of materials and structures.

Navier's work to derive continuum governing equations for a solid con-

taining numerous atoms could be regarded as the earliest dedication to connect lattice models with the mechanics of solids [113]. Later, Hrennikoff [52] and McHenry [83] worked on the inverse problem to approximate the elastic continuum model with a discrete spring-mass system. This idea resulted in the outgrowth of the finite element and finite difference methods.

1.1.1 Physical Lattices

Lattice models work best for the structures and materials naturally containing discrete units. Some examples illustrating this case are: space-fillers in architecture and civil engineering [39, 126], large space truss structures in aerospace engineering [26, 88], cellular foams [40] (Fig. 1.1 (a)), materials with negative Poisson’s ratios [67] and negative thermal expansion coefficients [105].

Over the last decade, a new class of ultra light weight materials called lattice materials (Fig. 1.1 (b) and (c)), has received increasing attention for its high stiffness-weight and strength-weight ratios [28, 112, 119, 122], energy absorption [36], shock mitigation [70] and heat insulation [62]. However, lattice materials bring a new type of mechanical problems. When the structure made of lattice materials is subjected to external loads, it fails locally at the structural unit level. To resolve all of the microstructures numerically is very challenging because the number of structural units in lattices could be up to millions or billions. The classical homogenization method is not a good prescription for such problems since the local response of the structural unit is

not considered in the equivalent continuum model.

1.1.2 Models Based on Lattices

The lattice model is a collection of one-dimensional bonds (elements) that interconnect at lattice sites (nodes), which are either regularly or irregularly situated in space [50]. Typically, there are two origins to approximate the bonds: (i) in the physics community, bonds are calculated from the interatomic potential energy (or strain energy); and (ii) in civil engineering, bonds are regarded as structural elements, such as trusses and beams. Therefore, lattices can be classified into two categories: atomic lattices and truss-like lattices.

The first category, atomic lattices (Fig. 1.1 (d)), is central to crystal physics [13–15, 59, 63, 64, 75]. The analysis of crystal defects such as dislocations and grain boundaries requires consideration of interatomic interactions on the scale of atomic lattices. The lattice statics and molecular dynamics provide powerful techniques to resolve atomic defects. The potential energy (or strain energy) of the deformed lattice is postulated with an empirical expression. In fact, numerous potentials with different levels of accuracy have been comprehensively investigated [17] in the molecular dynamics modeling field. For example, the simplest approximation of atomic interactions is the pair potential for which the potential energy only depends on the distances between two atoms. Popular pair potentials are the Lennard-Jones potential [3, 71, 97] and the Morse potential [66, 86]. Furthermore, the Lennard-Jones

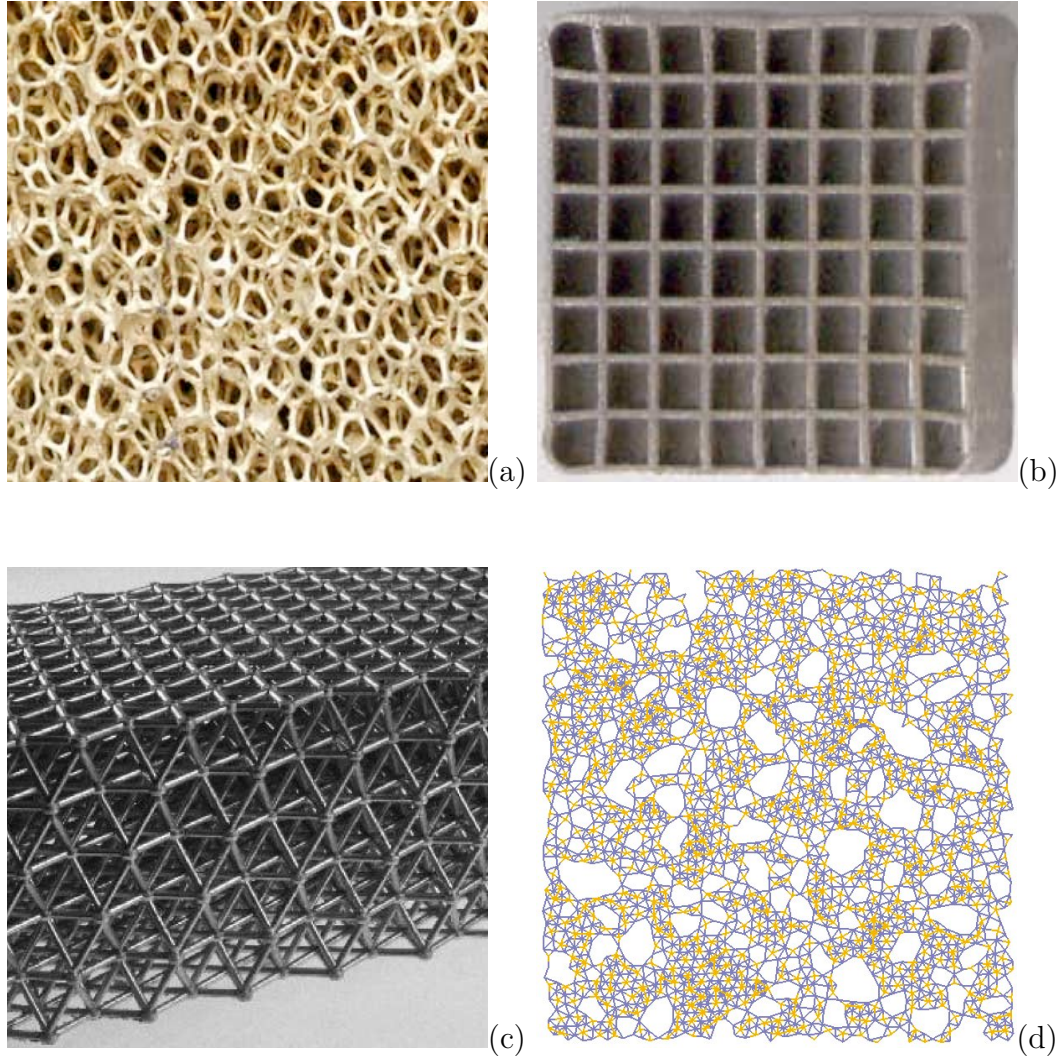


Figure 1.1: Representations of materials containing lattice structures: (a) Aluminum open-cell foam [55] ; (b) Cellular material [49] ; (c) Truss-like material [29] ; (d) Atomic network [103].

potential, for example, can be linearized around equilibrium positions based on the Cauchy-Born rule and reduced to the so-called harmonic potential. The resulting harmonic pair potential is equivalent to the Hookean spring (truss-like) lattice model [52]. However, under complex situations, such as surface reconstruction problems of solid crystals, the potential energy of bonds depends not only on distances of atoms, but also on actual positions or the local environment. For this reason, multibody potentials based on the embedded atom method [37, 85] and effective medium theory [53, 54] are utilized to resolve those problems.

The second category, truss-like lattices, can be viewed as continuum level counterparts of atomic lattice models. The one-dimensional interaction bonds in truss-like lattices are approximated by structural elements widely used in civil engineering, such as springs [48, 52, 91], trusses [7, 18] and beams [48, 51, 102, 115]. A very comprehensive discussion of the mechanics of lattice models has been given by Ostoja-Starzewski [90].

The application of both categories of lattices provides a practical way of discretizing continuum media. In particular, singular stress issues near the crack tip in continuum models are successfully avoided in lattices. Thus, lattice models are widely used to simulate fracture processes in atomic systems [1, 8, 22, 48, 50] and crack propagations in heterogeneous media. Examples of heterogeneous media include composites [92, 93], polycrystals [42, 91], soils [115], concretes [56, 102, 129], ceramics and rocks [7]. In Chapter 2 of this dissertation, we will describe a threshold resistance T -curve for subcritical

cracks based on the competition between crack rupture and healing. A kinetic Monte-Carlo lattice model is used to construct the threshold resistance T -curve in the absence of experimental data.

1.1.3 Solution Methods

In this dissertation, we are only concerned with the lattice statics, thus, solution methods for static problems will be presented in this section. The existing solution techniques can be typically classified into three categories [76]: brute force methods, homogenization and multiscale methods.

The first solution category, brute force methods, is particularly efficient when the system size of lattices is not too large. The microstructural details can be fully resolved in such methods. Approaches in this category include direct algorithms such as the structural analysis method and fast numerical algorithms such as FFT or multigrid [104].

The lattice analogue of the boundary element method or so-called boundary algebraic equations method [76, 79, 80] is one specific and powerful brute force approach. This method is similar to the classical boundary integral equation method, since algebraic equations defined on the boundary are used to replace the governing difference equation defined on the entire lattice. Boundary algebraic equations are formulated from the discrete fundamental solutions, called lattice Green's functions [78]. The approach of using boundary algebraic equations to replace difference equations for a regular lattice dates back to Saltzer [100]. This method offers a new way of using brute

force for model reduction on very large regular lattices, and its fast numerical implementations and strict error bounds are very attractive. Haq et al. [45, 46] presented some applications using boundary algebraic equations and the hybrid finite-boundary element method for problems on periodic lattices with interphases and defects. In Chapter 4 of this dissertation, we will discuss the applicability of lattice Green's functions as a multiscale modeling approach for solving problems defined on large-scale disordered lattices.

The second solution category, homogenization, is more suitable for the case when the local deformation is not important, and the global averaging response is desired. In addition, the system size could be very large. The mathematical theory of homogenization for media containing microstructures was well established since the nineteen sixties and seventies [10]. The literature closely associated with this asymptotic expansion homogenization for lattices includes the homogenization of reticulated structures [24], networks [116] and truss or frame lattices [77].

In the field of micromechanics, practical homogenization methods usually compute effective properties based on the energy equivalence in a repetitive unit cell between the lattice structure and the continuum model [27, 90, 91, 107]. Then, the continuum model with constant effective moduli can be solved using any conventional continuum discretization method. For disordered lattice models with strong heterogeneities, the global response can be achieved by the stochastic finite element approach [89, 95].

The third solution category, multiscale methods, is the prescription to

solve problems under two assumptions: (i) the system size is too large for available computational resources and (ii) an accurate solution is required only in a small subdomain, while the solution for the remaining region does not have to be accurate. This method addresses actual challenging problems, which include the mechanical analysis of lattice materials and crystal with defects. Multiscale methods for bridging diverse spatial scales are typically classified into two categories [23]: information passing approaches and concurrent approaches. In the concurrent schemes, models provide the simultaneous resolution of continuum and discrete length scales. In contrast, in the information-passing approaches, the parameters in the continuum model are extracted from the gross response of the microscopic model, and different models are solved sequentially. The major information passing approaches include the quasicontinuum method [110, 111], the equation free method [61], the heterogeneous multiscale method [32] and the generalized mathematical homogenization theory [23, 38]. The major concurrent approaches include the coupling of length scales [99], bridging domain [125] and bridging scale methods [96, 118]. In Chapter 3 of this dissertation, we will present multiscale analysis of large irregular lattices, and in particular with the use of classical continuum models for constructing accurate approximate solutions for boundary-value problems defined on such lattices.

1.2 Introduction of Anti-plane Elastostatic Lattices

In this dissertation, we mainly focus on lattices made of linear anti-plane elastostatic trusses as the underlying discrete model. Every node has one degree of freedom (out-of-plane displacement u). This anti-plane lattice model is equivalent to the elastic membrane, thermal conductivity and random fuse model, by virtue of mathematical analogies [2, 31, 114]. Examples of lattices with different topologies are illustrated in Figure 1.2.

For the anti-plane elasticity, Hooke's law for isotropic material is expressed as

$$\underline{\sigma} = \mu \underline{\gamma}. \quad (1.1)$$

The above notations for stresses and engineering strains are represented as: $\underline{\sigma} \equiv (\sigma_{31}, \sigma_{32})$ and $\underline{\gamma} \equiv (\gamma_{31}, \gamma_{32})$ in the $3D$ elasticity. μ is the shear modulus. The kinematic equations are

$$\underline{\gamma} = \nabla u, \quad (1.2)$$

where u denotes the out-of-plane displacement, and the equilibrium equations are

$$\nabla \underline{\sigma} = 0. \quad (1.3)$$

Combining the above equilibrium, kinematic and constitutive equations, we obtain the governing equation

$$\Delta u = 0, \quad (1.4)$$

which is the Laplace equation of the scalar u .

In the discrete setting, each lattice bar (or bond) with the shear modulus μ_0 is linked through two nodes i and j . The relationship of nodal displacements and forces transmitted by the bond is represented in the matrix form

$$\frac{\mu_0 A}{l} \begin{pmatrix} 1 & -1 \\ -1 & 1 \end{pmatrix} \begin{pmatrix} u_i \\ u_j \end{pmatrix} = \begin{pmatrix} f_i \\ f_j \end{pmatrix}. \quad (1.5)$$

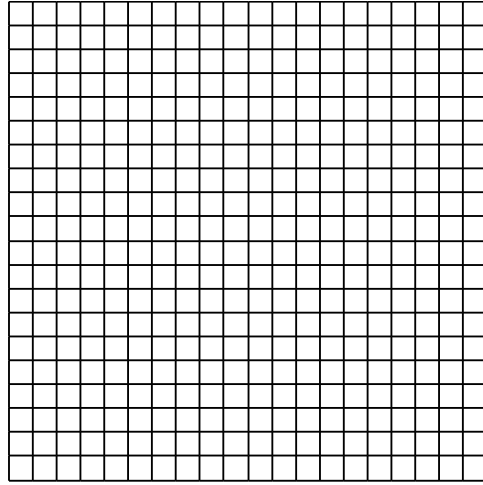
Here A and l are the cross-sectional area and length of the bar element, respectively. The symbols u_i and f_i denote the nodal displacement and force at the node i . Following the structural analysis procedure, the algebraic governing equations are assembled in the standard form

$$\mathbf{K}\mathbf{u} = \mathbf{f}. \quad (1.6)$$

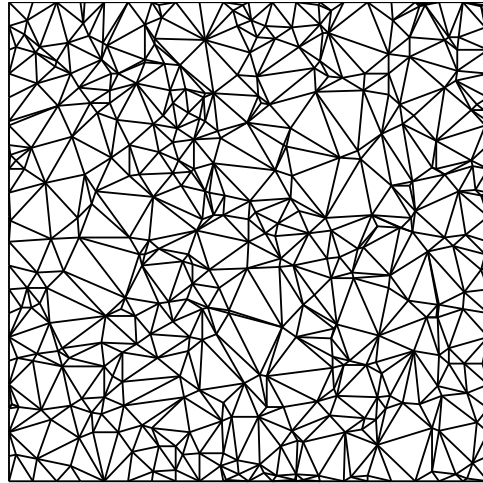
Here \mathbf{K} , \mathbf{u} and \mathbf{f} denote the global stiffness matrix, nodal displacements and forces, respectively. The equations of (1.6) are closed by prescribing displacements at the exterior boundary and forces in all other interior nodes, so that (1.6) provides a unique solution for the remaining displacements. The most straightforward solution method is to use the conventional structural analysis approach, which involves the procedure to assemble the global stiffness matrix \mathbf{K} and compute the inverse of \mathbf{K} .

1.3 Dissertation Structure

This dissertation is organized as follows. In the next three chapters, we will provide the elaboration of three modeling studies based on lattices. In the last chapter, we will summarize results and discuss future work. In the



(a)



(b)

Figure 1.2: Examples of lattices: (a) Square lattice; (b) Delaunay lattice.

remaining sections of this chapter, we will briefly introduce the three modeling studies based on lattices.

1.3.1 The Resistance Curve for Subcritical Cracks Near the Threshold

In Chapter 2, we generalize Rice’s work [98] by extending it to fracture specimens undergoing microstructural changes. This generalization qualitatively changes the threshold concept. In particular, it is demonstrated that microstructural changes give rise to multiple threshold states. One consequence of this conclusion is that the oscillatory crack behavior associated with a particular threshold state is preceded by a growth (or healing) stage. This is equivalent to saying that, in the presence of microstructural changes, the threshold concept is generalized by a T -curve similar to the way the fracture toughness concept is generalized by the R -curve. Towards this objective, a kinetic Monte-Carlo lattice model incorporating rupture and healing is used to construct the threshold resistance T -curve in the absence of experimental data. The material of Chapter 2 has been published in the International Journal of Fracture [128].

1.3.2 On Continuum Approximation of Irregular Lattices

In Chapter 3, we are concerned with multiscale analysis of large irregular lattices, and in particular with the use of classical continuum models for constructing accurate approximate solutions for boundary-value problems defined on such lattices. Accordingly, the lattice model is treated as exact (or

microscopic) and the continuum model as approximate (or macroscopic).

Our point of departure is that, for many problems associated with fracture and microscopic pattern formation, characterization of the continuum model is an important but nevertheless secondary objective. For those problems, the primary objective is to compute microscopic quantities relevant to the phenomenon of interest. Accordingly, we focus not on the continuum model but on how its introduction affects the microscopic quantities of interest. Furthermore, in contrast to the majority of multiscale models involving continuum components, we engage the continuum model not as a component of a multiscale model, but rather as a generator of a limited approximation basis for exact solutions of boundary-value problems defined for the exact lattice model.

1.3.3 On Extension of Boundary Algebraic Equations to Irregular Lattices

In Chapter 4, we attempt to extend boundary algebraic equations (BAEs) to irregular lattices. Such an extension would be indispensable for solving multiscale problems defined on irregular lattices, as BAEs provide a seamless transition to remote boundary conditions. We developed a BAE for a model problem relevant to analyzing defects in irregular lattices. Nevertheless, this BAE requires statistical treatment and certain terms of it are as difficult to compute as the solution itself. In contrast, for regular lattices, the BAE can be treated deterministically and the same terms are very easy to compute.

Thus, for now, the idea of applying BAEs to irregular lattices is not attractive. An appropriate statistical setting for this problem is very challenging and is not pursued here. In the end of this chapter, we summarize the difficulties associated with those BAEs and outline possible avenues for future research.

Chapter 2

The Resistance Curve for Subcritical Cracks Near the Threshold

Thermodynamic analysis of brittle fracture specimens near the threshold developed by J. R. Rice [Thermodynamics of quasi-static growth of Griffith cracks, *J Mech Phys Solid*, **26**, pp. 61-78, (1978)] is extended to specimens undergoing microstructural changes. The proposed extension gives rise to a generalization of the threshold concept that mirrors the way the resistance curve generalizes the fracture toughness. In the absence of experimental data, the resistance curve near the threshold is constructed using a basic lattice model.

2.1 Introduction

According to elementary fracture mechanics, rapid crack growth occurs when the Mode I stress intensity factor K exceeds its critical value K_c . In the subcritical regime $K < K_c$ crack growth is slow. Also it is widely accepted that growth stops completely for $K < K_{th}$. Under fixed ambient conditions, the threshold K_{th} is treated as a material property. It is important in many biomedical, chemical, geotechnical, and nuclear engineering applications.

According to the conventional definition, the condition $K < K_{th}$ implies that the crack velocity \dot{a} is zero no matter how long the specimen is exposed to loading. In reality, this assertion is validated only over a finite hold time and within a certain length resolution associated with crack growth. Note that a patient observer with an accurate measuring device is more likely to observe crack growth than a less patient observer with a less accurate measuring device. Thus patience and accuracy favor lower values of K_{th} . Ultimately, an infinitely patient observer with an infinitely accurate measuring device should report $K_{th} = 0$!

In practice, the threshold is associated with an extremely small rather than zero crack velocity. This is sufficient for estimating a lower bound for the time it takes to reach the critical state $K = K_c$. The usefulness of this approach is somewhat limited, especially for applications involving very large times. In this regard, it is instructive to examine some of available experimental data. Most of the data compiled in [69] are collected under conditions characterized by velocities in the range between 10^{-6} and 10^{-12} m/s . However, in a recent study [82], it is suggested that the velocity should be as low as 10^{-14} m/s . For current measuring devices, this velocity gives rise to the test duration close to one year [82]. For most applications, such a choice should be prohibitive. More importantly, there are no good reasons to believe that the resulting K_{th} is a material property.

A rigorous argument in favor of $K_{th} > 0$ has been made by Rice [98], who associated the threshold with a transition between growth and healing.

According to Rice, the crack fluctuates near the threshold, with healing being dominant in the regime $K < K_{th}$ and growth being dominant in the regime $K > K_{th}$. This behavior has been validated by Lawn and co-workers [120, 121] who conducted elegant experiments involving loading-unloading cycles leading to crack growth and healing. Unfortunately, by and large Rice's work remains ignored by practitioners. On the one hand, this could be easily explained by difficulties associated with registering healing. On the other hand, healing is ubiquitous in biological systems, and it has been observed in polymers [57, 58, 101, 124], ceramics [20, 25, 35, 44, 68, 123], concrete [54] and rocks [106]. Furthermore, several healing mechanisms have been identified, and among them healing by diffusion appears to be the most common one [19]. Here we distinguish between healing and toughening mechanisms. The latter make crack growth more difficult but do not lead to negative crack growth. Of course toughening mechanisms may interact with healing ones. In particular, we single out a universal zero-temperature toughening mechanism associated with statistical spatial inhomogeneity of the fracture toughness [12, 21].

The principal limitation of Rice's analysis is that it is restricted to brittle specimens. In this chapter, we remove this limitation by taking into account microstructural changes due to creep. This generalization qualitatively changes the threshold concept. In particular, we demonstrate that microstructural changes should result in a threshold spectrum rather than a single threshold value. As far as the macroscopic behavior is concerned, this proposition implies that in general the threshold state may be preceded by

a growth (or healing) stage. This behavior mirrors that of the R -curve [16], in which K_c is treated as a function of the crack advance Δa rather than a constant. Accordingly, we refer to the threshold spectrum as the T -curve.

We are not aware of any experimental data suitable for validating (or invalidating) our proposition because the current practice of data reporting does not include the function $\Delta a(t)$, which is critical for constructing the T -curve. As a partial remedy, we introduce a very basic lattice model which allows us to construct synthetic data and compute the T -curve.

The rest of the chapter is organized as follows. In Section 2.2, following Rice [98], we analyze fracture specimens undergoing microstructural changes. In Section 2.3, we introduce the lattice model. In section 2.4, we present simulation results. In section 2.5, we summarize key results of our work.

2.2 Analysis

In this section, we consider a hypothetical threshold test conducted on a clamped Mode I fracture specimen (Fig. 2.1) subjected to a step load. We assume that the specimen is infinite, the crack is semi-infinite, and inelasticity is confined to a small zone adjacent to the crack tip, so that the energy release rate G remains constant throughout the test.

In the absence of microstructural changes, the threshold is described by the inequality [98]

$$(G - 2\gamma) \dot{a} \geq 0 \tag{2.1}$$

where γ is the specific surface energy. This inequality implies growth for $G - 2\gamma > 0$ and healing for $G - 2\gamma < 0$. We regard a as the external (observable) state variable and $G - 2\gamma$ as the conjugate thermodynamic force. The threshold is associated with the equilibrium condition $G - 2\gamma = 0$, with the implication that this equilibrium state is stable.

In the presence of microstructural changes, (2.1) is generalized as

$$\left[\hat{G}(G, \phi) - 2\gamma \right] \dot{a} + \boldsymbol{\lambda} \cdot \dot{\boldsymbol{\phi}} \geq 0 \quad (2.2)$$

Here ϕ is a column vector of internal (non-observable) state variables representing the microstructure and $\boldsymbol{\lambda}$ is a column vector of thermodynamic forces conjugate to ϕ . The hat symbol is used to emphasize that the energy release rate depends on microstructural details, and the macroscopic energy release rate G is treated as a loading parameter.

In the presence of microstructural changes, one cannot make a conclusive statement about the sign of \dot{a} unless the internal state has been equilibrated. With this provision, (2.2) reduces to the familiar inequality structure

$$\left[\hat{G}(G, \phi^*) - 2\gamma \right] \dot{a} \geq 0. \quad (2.3)$$

Here ϕ^* denotes stable equilibrium states. Inequality (2.3) implies that each pair (G, ϕ^*) satisfying

$$\hat{G}(G, \phi^*) - 2\gamma = 0 \quad (2.4)$$

can be regarded as a threshold state. Thus it becomes appropriate to consider a threshold spectrum rather than a single threshold value.

Let us rewrite (2.4) in a form that does not include explicit dependence on the internal state. To this end, we assume that (2.4) can be solved for G and expressed in the form

$$G - \hat{G}_{th}(\phi^*) = 0, \quad (2.5)$$

so that explicit dependence on the internal state is transferred to the state function $\hat{G}_{th}(\phi^*)$. Next, we observe that for each pair (G, ϕ^*) satisfying (2.4) there exists a corresponding Δa^* . This allows us to rewrite (2.5) in the form

$$G - G_{th}(\Delta a^*) = 0 \quad (2.6)$$

which does not include explicit dependence on the internal state. We refer to the function $G_{th}(\Delta a^*)$ as the T -curve. It is straightforward to determine experimentally, as it represents all pairs $(G, \Delta a^*)$ associated with macroscopic thermodynamic equilibrium.

The T -curve shares many common features with the R -curve widely used for representing plasticity effects on the fracture toughness [16]. The idea behind the R -curve is that the plastic flow near the crack tip produces an additional toughening effect as the crack grows. However, at some point, the plastic flow becomes steady and the effective toughness reaches a steady value. As a result the function $G_c(\Delta a)$ initially increases and then reaches a plateau. It is reasonable to expect that the T -curve behaves similarly, although the toughening effect is expected to be associated with creep rather than plasticity.

Similarly to the R -curve, the usefulness of the T -curve is limited because it is constructed under constant G conditions, and for most specimens

G depends on a . This dependence may significantly affect the evolution of the internal state, and ultimately the equilibrium states forming the threshold spectrum. Thus the use of the T -curve should be restricted to small Δa^* .

It is worth emphasizing one major difference between the conventional and proposed threshold testing. In the standard test, the apparent value of G_{th} is lower for patient observers. In contrast, in the proposed approach, a patient observer is rewarded with a high value of G_{th} because the time to reach equilibrium should be large for large G . In this regard, an intriguing question is whether the T -curve approaches G_c for large Δa^* .

It is instructive to compare the restrictions imposed on the crack growth in the conventional, Rice's, and proposed approaches. The conventional approach is characterized by the restrictive condition

$$\Delta a = 0 \quad \text{for all } t > 0.$$

The other two approaches require the introduction of the average crack growth increment

$$\overline{\Delta a}(t) := \frac{1}{t} \int_0^t \Delta a(t') dt'.$$

Then, according to Rice, the conventional restriction is relaxed as

$$\overline{\Delta a}(t) \rightarrow 0 \quad \text{as } t \rightarrow \infty.$$

Finally, the proposed approach involves the most relaxed condition

$$\overline{\Delta a}(t) \rightarrow \Delta a^*(G) = G_{th}^{-1}(G) \quad \text{as } t \rightarrow \infty. \quad (2.7)$$

2.3 Simulation Methodology

In this section, we present a methodology for computing the T -curve using a model specimen well suited for simulations.

2.3.1 Specimen Description

In the previous section, the T -curve was introduced using an infinite clamped specimen with a semi-infinite crack. For simulation purposes, it is neither necessary nor useful to consider the entire specimen. Instead we consider its process zone subjected to boundary conditions consistent with the K -fields. Furthermore, all arguments presented in the previous section for Mode I specimens also hold for Mode III specimens, which are easier to simulate than their Mode I counterparts.

For simulations, we consider specimens similar to the one shown in Figure 2.2. Each specimen microstructure is a simple square lattice whose nodes have the Cartesian coordinates

$$x_1 = li_1 \quad \text{and} \quad x_2 = l \left(i_2 + \frac{1}{2} \right)$$

where l denotes the lattice spacing, and i_1 and i_2 are integers (Fig. 2.2). The lattice microstructure is well suited for simulations, especially those involving microstructural changes associated with rupture and healing of its bonds; a model describing those processes will be presented in Section 2.3.2. The macroscopic specimen dimensions are such that the crack length is equal to Ml , the size along the x_1 axis is equal to $2Ml$, and the size along the x_2 axis

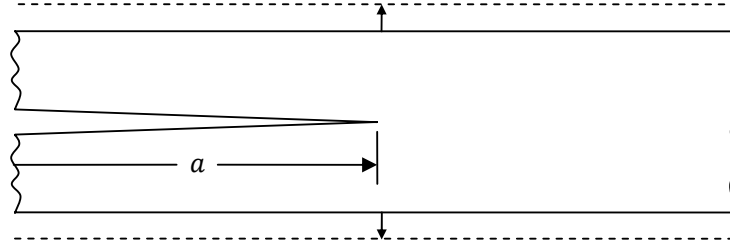


Figure 2.1: Clamped Mode I fracture specimen.

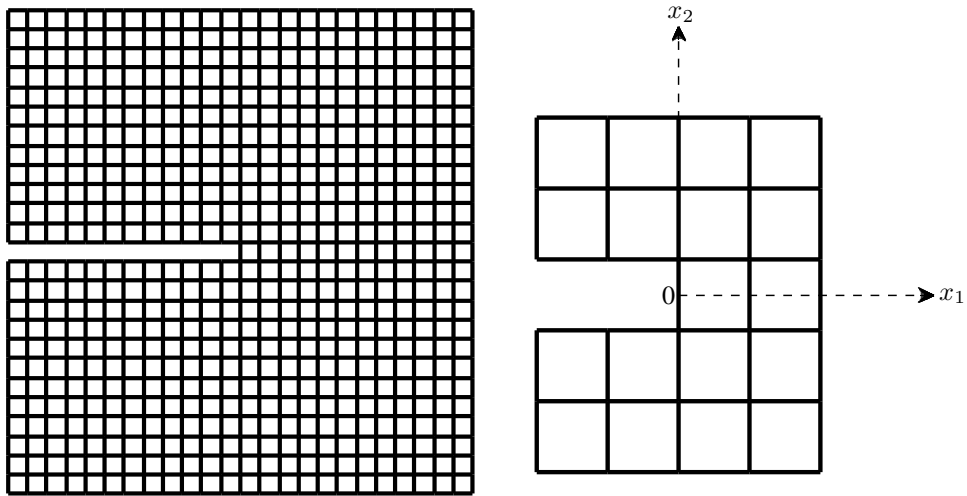


Figure 2.2: The fracture specimen for $M = 12$ (left); The crack tip and the coordinate system (right).

is equal to $(2M + 1)l$. Ultimately, M must be chosen sufficiently large, so that all quantities of interest, and in particular the T -curve, are independent of M .

Under anti-plane deformation, the elastic response of a bond is governed by the stiffness c relating the shear force per unit out-of-plane thickness and the difference between the out-of-plane nodal displacements. On the macroscopic scale, the overall elastic response is represented by the overall shear modulus

$$\mu = c$$

This relationship is straightforward to establish by considering a periodic problem for an $l \times l$ cross.

The specimen is loaded by prescribing the Mode III displacements [16]

$$u(r, \theta) = \sqrt{\frac{Gr}{\pi\mu}} \sin \frac{\theta}{2} \quad (2.8)$$

at the exterior nodes, except for the nodes on the crack faces; all other nodes are kept force-free. Here r and θ are the polar coordinates (Fig. 2.2b). We regard G as the loading parameter.

The adopted model is known in the literature as a random fuse model; for pertinent details and a literature survey we refer to a comprehensive review [2].

2.3.2 Bond Rupture and Healing

We assume that lattice bond rupture is a thermally activated process and adopt a commonly used model for this phenomenon [9]. In that model it

is assumed that an infinitesimal probability of rupture $\delta\Phi$ under a *constant* force F during an infinitesimal time interval $(t, t + \delta t)$ is given by the equation

$$\delta\Phi = \Psi(t, F) \exp\left(\frac{F}{R}\right) \frac{\delta t}{\tau}. \quad (2.9)$$

Here Ψ is the probability of survival in the time interval $(0, t)$; R and τ are model constants. During the time interval $(t, t + \delta t)$ the probability of survival is reduced by $\delta\Phi$,

$$\Psi(t + \delta t, F) - \Psi(t, F) = -\delta\Phi, \quad (2.10)$$

so that we can combine (2.9) and (2.10) to obtain

$$\Phi(t, F) = 1 - \exp\left[-\exp\left(\frac{F}{R}\right) \frac{t}{\tau}\right] \quad (2.11)$$

and

$$\Psi(t, F) = \exp\left[-\exp\left(\frac{F}{R}\right) \frac{t}{\tau}\right]. \quad (2.12)$$

Let us emphasize that these simple expressions are valid only when F is held constant. In general, the solution of (2.9) and (2.10) requires numerical integration. Also note that the probability of survival approaches zero exponentially fast as t and F increase. Thus (2.9) is close to the rule that states that a bond ruptures once the force reaches a critical value.

According to the chosen rupture model, even unloaded specimens will eventually fail. To prevent this from happening, we assume that the probability of healing of a vacant site during the time interval $(t, t + \delta t)$ is given by the equation

$$\delta\Pi = \alpha [1 - \Pi(t)] \frac{\delta t}{\tau}, \quad (2.13)$$

where α is a dimensionless material constant. This equation parallels (2.9) as the term $1 - \Pi$ represents the probability of non-healing in the time interval $(0, t)$. Upon integration of (2.13) we obtain

$$\Pi(t) = 1 - \exp\left(-\frac{\alpha t}{\tau}\right). \quad (2.14)$$

2.3.3 Implementation Details

In a typical numerical experiment, a specimen similar to that shown in Figure 2.2 was subjected to Mode III displacement-prescribed boundary conditions (2.8), with G held constant throughout the experiment. Due to microstructural changes, an incremental computational procedure was necessary. In that procedure, each increment was associated with one and only one microstructure changing event. To explain the procedure we use the induction, and suppose that an event occurs at a certain time $t = t_0$. Using this information, we have to determine (i) the time $t_0 + \Delta t$ when the next event occurs and (ii) the event itself.

First, we determine the forces transmitted by the bonds of the instantaneous microstructure by solving equations governing the elastic response. Those equations combine the force equilibrium and Hooke's law. For example, for a node attached to four bonds the governing equation is the well-known five-point stencil

$$c[4u(i_1, i_2) - u(i_1 + 1, i_2) - u(i_1 - 1, i_2) - u(i_1, i_2 + 1) - u(i_1, i_2 - 1)] = f(i_1, i_2) \quad (2.15)$$

Here i_1 and i_2 are integer coordinates, u is the nodal displacement, and f is the nodal force. If the number of bonds is less than four, then (2.15) must be modified. For example, if the bond between the nodes (i_1, i_2) and $(i_1 + 1, i_2)$ is missing, then (2.15) is modified as

$$c[3u(i_1, i_2) - u(i_1 - 1, i_2) - u(i_1, i_2 + 1) - u(i_1, i_2 - 1)] = f(i_1, i_2)$$

Nodes not attached to at least one bond are disregarded. The system of algebraic equations is closed by setting $f = 0$ at every node except for the boundary nodes where the displacements are prescribed.

Once the forces have been determined, the time increment Δt toward the next event and the event itself can be computed using kinetic Monte-Carlo method [117], [127], [84]. Here, we closely follow the scheme used in [73] and [33]. Suppose that there are m bonds and n vacancies and the local time scale is set so that $t_0 = 0$. The probability that an event occurs during an infinitesimal time interval $(\Delta t, \Delta t + \delta t)$ but not during a finite time interval $(0, \Delta t)$ is expressed as

$$\delta P = N(\Delta t) \left[n\alpha + \sum_{i=1}^m \exp\left(\frac{F_i}{R}\right) \right] \frac{\delta t}{\tau}. \quad (2.16)$$

Here $N(\Delta t)$ is the probability of no event occurring during the finite time interval $(0, \Delta t)$. Note that the probabilities of the independent events involved in this equation are infinitesimal, and therefore the usual rules of probability theory can be replaced with simple addition. Following (2.10), during the infinitesimal time interval $(\Delta t, \Delta t + \delta t)$, the probability N is reduced by δP ,

so that

$$\delta P = -[N(\Delta t + \delta t) - N(\Delta t)] = -\frac{\partial N(\Delta t)}{\partial t} \delta t. \quad (2.17)$$

Now we can combine (2.16) and (2.17) into the ordinary differential equation

$$\frac{\partial N(\Delta t)}{\partial t} = -N(\Delta t) \left[n\alpha + \sum_{i=1}^m \exp\left(\frac{F_i}{R}\right) \right] \frac{1}{\tau}$$

with the initial condition is $N(0) = 1$. This equation is easy to integrate over the time interval $(0, \Delta t)$ because on this interval the forces remain constant.

As a result we obtain

$$N(\Delta t) = \exp \left\{ - \left[n\alpha + \sum_{i=1}^m \exp\left(\frac{F_i}{R}\right) \right] \frac{\Delta t}{\tau} \right\}. \quad (2.18)$$

This equation can be used to solve for the time increment Δt , by equating $N(\Delta t)$ to a realization of a random variable uniformly distributed over the interval $(0,1)$.

Once the time increment Δt has been determined, the corresponding microstructural event is chosen according to the following three-step procedure:

- Assign the probability for each individual rupture event, $1 \leq k \leq m$,

$$w_k = \frac{\exp\left(\frac{F_k}{R}\right)}{n\alpha + \sum_{i=1}^m \exp\left(\frac{F_i}{R}\right)};$$

- Assign the same probability to all healing events, $m+1 \leq k \leq m+n$,

$$w_k = \frac{\alpha}{n\alpha + \sum_{i=1}^m \exp\left(\frac{F_i}{R}\right)};$$

- Among the $m + n$ events, the chosen one has the number i , determined by the inequality

$$\sum_{j=1}^{i-1} w_j \leq \eta \leq \sum_{j=1}^i w_j$$

where η is a realization of a random variable uniformly distributed over the interval $(0,1)$. If $\eta < w_1$ then $i = 1$.

For our purposes, it is important to differentiate between events associated with crack growth versus damage accumulation. To this end, we adopt the following rules for constructing the function $a(t)$:

- Throughout the loading history, the crack is defined as a contiguous path of ruptured bonds starting at the origin. The crack length is defined as the path projection on the x_1 -axis. For example, if rupture occurs in the bonds centered at $(0,0)$ and $(l,0)$, then the crack increment $\Delta a = 2l$. However, if rupture occurs in the bond centered at $(l,0)$ but the bond centered at $(0,0)$ is intact, then $\Delta a = 0$.
- For the original vacancies, introduced to form the crack, healing is allowed only for the vacancy centered at $(-l,0)$. If that vacancy has healed, then healing is allowed only for the vacancy centered at $(-2l,0)$, and so on.
- Healing of vacancies created throughout the loading history is dictated by (2.13), without any additional restrictions.

2.4 Simulation Results

In this section, we present simulation results obtained using the methodology described in Section 2.3. The simulation objective is to construct the T -curve and to examine associated statistical and size effects. The structure of the governing equations is such that all simulation results can be normalized so that α becomes the only important model parameter.

2.4.1 Crack Growth Versus Damage Accumulation

In this section, we examine the competition between crack growth (or healing) versus damage accumulation. Crack growth is driven by rupture of a small number of bonds ahead of the crack tip, whereas damage accumulation is driven by rupture away from the crack tip. Since the probability of rupture is an exponential function of G (2.11), high values of G (load) favor crack growth rather than damage accumulation. Thus, for a fixed α , the rupture pattern represents damage accumulation for low G , and straight crack growth for high G . In between, one can observe various combinations of crack growth and damage accumulation, including curvilinear crack paths (Fig. 2.3). Near a threshold, $\alpha \gg 1$ requires relatively large G_{th} , and therefore thresholds corresponding to $\alpha \gg 1$ favor crack growth rather than damage accumulation. Consequently, one can simulate thresholds corresponding to $\alpha \gg 1$ using relatively small specimens. Therefore simulation results presented in this chapter involve $\alpha \gg 1$.

Let us emphasize that, in this chapter, we are concerned with con-

structing a meaningful T -curve by identifying a sufficiently large specimen size M rather than by characterizing the process zone surrounding the crack tip. Therefore a detailed analysis of the process zone is not required. Thus our approach parallels that leading to the restriction on the minimum specimen size for fracture toughness testing [16]:

$$L_{min} \geq 2.5 \left(\frac{K_c}{\sigma_y} \right)^2 ,$$

where σ_y is the yield stress, and the factor 2.5 is determined empirically. This factor is determined without relying on any particular process zone model.

2.4.2 Quasi-brittle Regime

In this section, we analyze the asymptotic regime as $\alpha \rightarrow \infty$. In this regime, rupture events are limited to the bond ahead of the crack tip, and healing events are limited to the vacancy right behind the crack tip. As a result the threshold state is characterized by fluctuations between rupture of that bond and healing of that vacancy. By equating the probabilities of these events,

$$\exp \left(\frac{F}{R} \right) = \alpha ,$$

one obtains the force in the bond ahead of the crack tip

$$F = R \log \alpha .$$

For the specimen shown in Figure 2.2, this force corresponds to displacement boundary conditions (2.8) governed by

$$G = 1.26 \frac{R^2}{cl} \log \alpha^2 \tag{2.19}$$

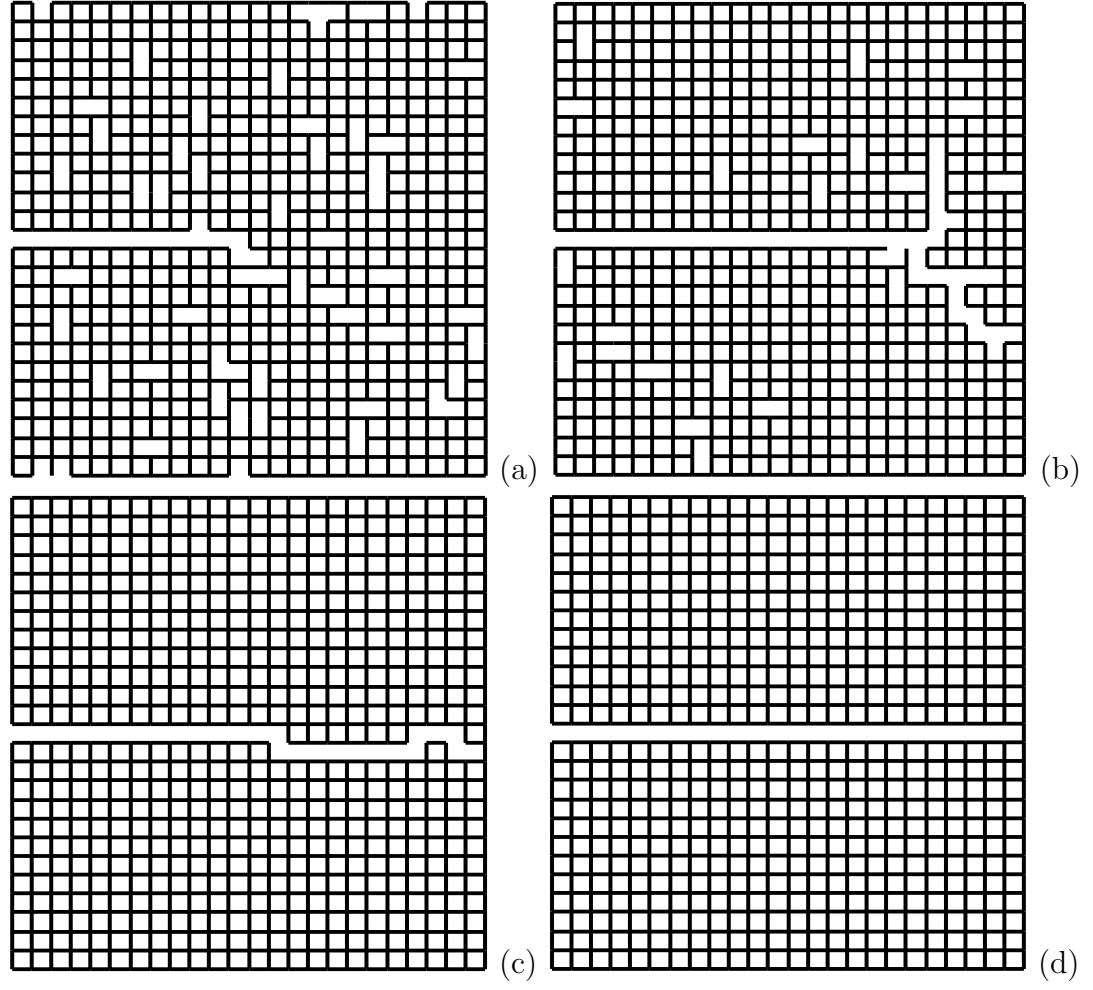


Figure 2.3: Rupture patterns for $\alpha = 100$ and $M = 12$: (a) Damage accumulation for $G = 1.02G_B$; (b) Damage and crack growth for $G = 7.97G_B$; (c) Curvilinear crack growth path for $G = 15.3G_B$; (d) Straight crack growth path for $G = 40.0G_B$.

Here the numerical factor is determined computationally. Equation (2.19) is regarded as an asymptotic estimate for the threshold for $\alpha \gg 1$.

It is worth mentioning that in the asymptotic regime the specimen behaves as if it were brittle because the strong healing effectively freezes microstructural events in the bulk of the specimen. Accordingly, we denote G defined in (2.19) by G_B where the subscript B refers to brittle:

$$G_B = 1.26 \frac{R^2}{cl} \log \alpha^2$$

There is another parallel with brittle behavior, as in the asymptotic regime G_B is the only threshold value. Indeed, in this regime, $G > G_B$ leads to unbounded crack growth, whereas $G < G_B$ leads to unbounded crack healing. The corresponding T -curve has the form

$$G_{th}(\Delta a) = G_B H(\Delta a)$$

where H is Heavyside's step function. Of course for $\Delta a > 0$ this is the form of the R -curve for rapidly growing cracks.

2.4.3 T -curve

In this section, we present simulation results for the T -curve. Simulation results are presented by normalizing Δa by l , the time t by τ , and G by G_B . In particular, we express the function $G_{th}(\Delta a^*)$ as

$$G_{th}(\Delta a^*) = G_B \mathcal{F} \left(\alpha, \frac{\Delta a^*}{l} \right) . \quad (2.20)$$

Thus our objective is to construct the dimensionless function \mathcal{F} of two dimensionless variables. This function must be independent of the specimen size M . Also it is important to examine the significance of statistical effects.

Equilibrium states were computed according to the following rules:

1. From numerical experiments, it was established that a typical transient growth (or healing) stage involves about 5,000 events and its duration is close to $t = \tau$;
2. A typical simulation lasted for $t = 5\tau$.
3. The mean and the standard deviation for the function $\overline{\Delta a}(t)$ were computed over the interval $2\tau \leq t \leq 5\tau$;
4. The mean was accepted as Δa^* as long as the standard deviation was less than 1% of the original crack length Ml .
5. Rejections were associated with specimen breaking and were treated as simulation artifacts.

Simulation results for the T -curve for $\alpha = 100$ using specimens with $M = 8$ and $M = 12$ are presented in Figure 2.4. To avoid numerical artifacts associated with specimen breaking, simulation were restricted to $\Delta a^* \leq .5Ml$. The data for $M = 8$ and $M = 12$ are in the range of Δa^* where comparisons are meaningful, and therefore the size effect appears to be small. The T -curve is well approximated by a straight line with the intercept $G_{th}(0) \approx G_B$.

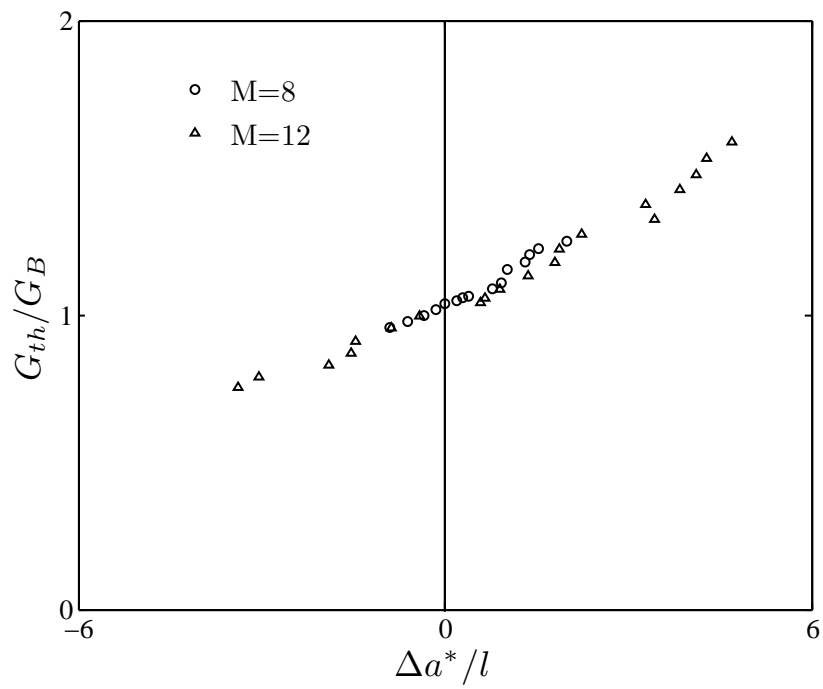


Figure 2.4: The T -curve for $\alpha = 100$ using specimens with $M = 8$ and $M = 12$.

To examine statistical effects, we conducted simulations for $\alpha = 100$ using specimens with $M = 8$ and $M = 12$. We selected two values of G for each specimen size, and computed ten realizations per G . In each case, the standard deviation for Δa^* was less than a half of the lattice spacing. For small Δa^* , this value of the standard deviation may represent significant size effects. Nevertheless, its significance is greatly reduced for large $|\Delta a^*|$. This behavior is not surprising, as for large $|\Delta a^*|$, one expects that equilibrium is controlled by a large number of rupture and healing events in the bulk of the specimen rather than a small number of events near the crack tip.

We also examined the dependence of \mathcal{F} on α , with an expectation that the dependence of G_{th} on α is captured by G_B . To this end, we computed \mathcal{F} for $M = 12$ and $\alpha = 50, 100, 1000$ and determined that there is a weak dependence of \mathcal{F} on α .

Finally, we examined memory effects. In particular, we considered two loading histories for $\alpha = 100$ and $M = 12$:

$$G_1(t) = 0.87G_B H(t) + .5G_B H(t - 2\tau)$$

and

$$G_2(t) = 1.37G_B H(t) - .5G_B H(t - 2\tau)$$

for $t \leq 12\tau$. If memory effects were absent, then one would expect that the first history would result in the same Δa^* as the history $G = 1.37G_B H(t)$, whereas the second history would result in the same Δa^* as the history $G = 0.87G_B H(t)$. In contrast, the simulation results were $\Delta a_1^* = 2.44l$ versus $3.28l$

and $\Delta a_2^* = -0.57l$ versus $-1.53l$. That is, in both cases, the initial stage mattered. For the first history, it resulted in reduced growth in comparison to the reference history $G = 1.37G_B H(t)$. Similarly, for the second history, the initial stage resulted in reduced healing in comparison to the reference history $G = 0.87G_B H(t)$. In summary, the adopted model predicts significant history effects.

2.5 Closure

In this chapter, we extended thermodynamic analysis of brittle fracture specimens near the threshold developed by Rice (1978) to specimens undergoing microstructural changes. Key conclusions of this work are as follows:

- In order to achieve a non-zero threshold value, the healing mechanism should be taken into account. (Here, we single out crack closure as a different mechanism to affect the threshold.)
- In the presence of healing and microstructural changes, one should expect multiple threshold states.
- On the macroscopic level, the multiple threshold states can be represented by a T -curve, which is quite similar to the R -curve.

In the absence of necessary experiments, the T -curve was constructed using a basic lattice model. Although the adopted model can be easily criticized as unrealistic, its basic feature, involving the competition between rupture and

healing, could be incorporated into a cohesive zone model. Such a construction is transparent, but the ensuing model is not expected to yield qualitatively different results.

Chapter 3

On Continuum Approximation of Irregular Lattices

3.1 Introduction

This chapter is concerned with multiscale analysis of large irregular lattices, and in particular with the use of classical continuum models for constructing accurate approximate solutions for boundary-value problems defined on such lattices. Accordingly, the lattice model is treated as exact (or microscopic) and the continuum model as approximate (or macroscopic). This topic is thoroughly understood for infinite periodic lattices governed by linear algebraic equations. In particular, there is a systematic procedure for constructing a hierarchy of continuum models from the equations governing the lattice model [77]. The first model in that hierarchy represents lattice symmetry but not its dimensions, whereas more complex models represent both. In principle, one can use that procedure to derive any known linear continuum model from an infinite periodic lattice. In contrast, finite irregular lattices do not lend themselves to elegant mathematical treatment, and therefore their analysis has to involve computational experiments. Nevertheless, required computing is straightforward, and it allows one to develop a good understanding of various important issues.

The most basic continuum model corresponding to an irregular lattice can be constructed by assuming that there is a mesoscopic representative volume element (RVE), whose extrinsic properties are adopted as intrinsic material properties of the macroscopic continuum model [47]. This point of view is widely accepted, and there is a very large body of literature dedicated to the determination of RVE properties. For irregular lattices, we single out the work of Ostoja-Starzhevski and Wang [94] who carried out Monte-Carlo simulations focused on statistical and size effects for RVEs representing three classes of two-dimensional lattices. In particular, those researchers determined the minimum RVE size l_0 for which classical elasticity model is acceptable within a prescribed tolerance ϵ .

Our point of departure is that, for many problems associated with fracture and microscopic pattern formation, characterization of the RVE is an important but nevertheless secondary objective. For those problems, the primary objective is to compute microscopic quantities relevant to the phenomenon of interest. Accordingly, we focus not on the continuum model but on how its introduction affects the microscopic quantities of interest. Furthermore, in contrast to the majority of multiscale models involving continuum components, we engage the continuum model not as a component of a multiscale model, but rather as a generator of a limited approximation basis for exact solutions of boundary-value problems defined for the exact lattice model.

A basic setting for our work involves a large irregular lattice Ω containing a small domain of interest ω , for which the displacements and forces must

be computed within a prescribed tolerance ϵ . We treat the lattice as a system responding to an input ϕ by an output ψ . We associate the input and output with nodal displacements at the exterior nodes $\partial\Omega$ and $\partial\omega$, respectively. In this context, our objective is to determine a family of inputs ϕ_0 for which the corresponding outputs ψ_0 are accurately approximated by the continuum model. It is argued that such inputs are characterized by a minimum wave length λ_0 dependent on tolerance ϵ .

Despite significant differences in problem settings and objectives, our approach has been significantly influenced by the work of Babuska and co-workers on pollution errors [6] and more recently on the penetration function [5]. Furthermore, our work supports their notion that one must be extremely careful in replacing microscopic models with macroscopic ones.

The remainder of the chapter is organized as follows. In Section 3.2 we formulate the problem. In Section 3.3 we analyze the problem using the singular value decomposition (SVD). In Section 3.4, we discuss simulation results. In Section 3.5, we discuss key results, their place in the pertinent literature, and propose avenues for further research. Mathematical tools used in this chapter are well established; we refer to [109] for details.

3.2 Problem Formulation

Consider a two-dimensional irregular lattice constructed according to the following procedure: (i) the nodes are generated as a set of points whose cartesian coordinates are uniformly distributed random variables, and (ii) the

nodes are connected by the bonds following the Delaunay triangulation. We refer to such lattices as Delaunay random lattices. This class of lattices were part of numerical experiments carried out in [94]. A convenient macroscopic parameter for such lattices is the areal node density μ . Throughout the paper we use the length $\sqrt{1/\mu}$ as the length gauge. Alternatively, one could use the average bond length h as the gauge. Monte-Carlo simulations provide a simple relationship between these two quantities:

$$h \approx \frac{1.15}{\sqrt{\mu}}.$$

A circular lattice is constructed by taking a large lattice and discarding all nodes lying outside of the circle and all bonds connected to at least one node lying outside of the circle. The exterior nodes of a lattice are defined as the set of vertices of the largest polygon whose edges are lattice bonds.

We assume that the lattice is subjected to anti-plane deformation and its bonds exhibit linear elastic behavior characterized by the stiffness inversely proportional to the bond length. This dependence is consistent with the assumption that all bonds have the same shear modulus and in-plane thickness.

Let us consider a circular lattice Ω of radius R . The lattice is subjected to prescribed displacements at the exterior nodes $\partial\Omega$, while the rest of the nodes are unloaded; we denote the vector of prescribed displacements by ϕ . This prescription gives rise to a well-posed linear algebraic problem, whose solution yields nodal displacements and internal forces in the lattice. This basic approach is applicable to sufficiently small lattices only.

For large lattices, one needs to develop a multiscale representation that delivers accurate predictions for the quantities of interest using significantly reduced amounts of data and arithmetic operations. We define the domain of interest ω as a circle of radius r ($r < R$) concentric with Ω . We define as the quantities of interest the nodal displacements of $\partial\omega$ and denote them by $\boldsymbol{\psi}$. By restricting the quantities of interest to the boundary, we suppose that all other nodal displacements of ω are less prone to errors associated with multiscale representation. The matrix relating the input $\boldsymbol{\phi}$ to the output $\boldsymbol{\psi}$ is referred to as the transmission matrix:

$$\boldsymbol{\psi} = \boldsymbol{T}\boldsymbol{\phi}. \quad (3.1)$$

This dimensionless matrix is uniquely defined by the lattice geometry.

Following the structure of multiscale models involving discrete and continuum components [72], we partition Ω into three concentric domains (Fig. 3.1):

- Domain of interest ω (circle of radius r);
- Deterministic buffer zone (ring with radii r and $\rho = r + \delta$);
- Statistical buffer zone (ring with radii ρ and R).

In a typical multiscale model involving discrete and continuum components, these zones are represented by the discrete, handshake, and continuum components, respectively. We depart from this representation by regarding the lattice

geometry as a deterministic entity in the domain of interest and deterministic buffer zone. In the statistical buffer zone, the lattice geometry is regarded as a statistical entity, but its areal node density μ is fixed and equal to that in the domain of interest and deterministic buffer zone. Thus, on the macroscopic scale, the lattice is uniform. In simulations, at first, the entire lattice is generated as a Delaunay random lattice. Then, the nodes inside the domain of interest and deterministic buffer zone are retained, whereas the nodes inside the statistical buffer zone are generated anew. The adopted structure of the statistical buffer zone is consistent with the view that the continuum model can be derived via ensemble averaging. Also, it is appropriate to treat the transmission matrix as a random variable, and focus on computing its mean value $\bar{\mathbf{T}}$ via ensemble averaging.

3.3 Singular Value Decomposition

The singular value decomposition theorem is a natural way of evaluating the transmission matrix:

$$\bar{\mathbf{T}}_{m \times n} = \mathbf{U}_{m \times m} \mathbf{S}_{m \times n} \mathbf{V}_{n \times n}^* . \quad (3.2)$$

Here the asterisk denotes matrix transposition. The matrix dimensions $m \times n$ represent the number of nodes of $\partial\omega$ and $\partial\Omega$, respectively; of course $m < n$. The matrices \mathbf{U} and \mathbf{V} are unitary ($\mathbf{U}^{-1} = \mathbf{U}^*$ and $\mathbf{V}^{-1} = \mathbf{V}^*$). The matrix \mathbf{S} is rectangular and consists of two blocks. The left block is a diagonal $m \times m$ matrix containing the singular values s_i , and the right block is an

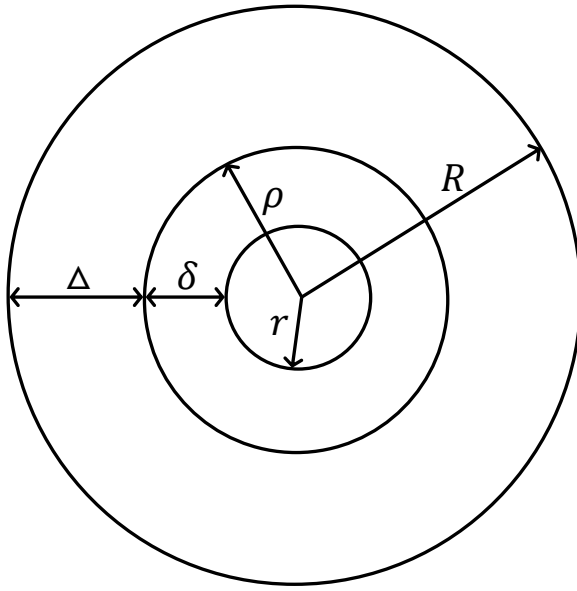


Figure 3.1: Circular lattice Ω (circle of radius R) and its subdomains: Domain of interest ω (circle of radius r); Deterministic buffer zone (ring with radii r and $\rho = r + \delta$); Statistical buffer zone (ring with radii ρ and R).

$m \times n - m$ matrix filled with zeros. The singular values are numbered so that $s_1 \geq s_2 \geq \dots \geq s_m$.

The singular value decomposition theorem lends itself to a transparent and useful interpretation, once we regard ϕ as an input and ψ as the corresponding output. Then the vector $\mathbf{V}^* \phi$ represents the input as a superposition of n orthogonal inputs. The structure of the matrix \mathbf{S} implies that out of n of those inputs only the first m are transmitted; the singular values represent the weights assigned to those m inputs. Finally, the matrix \mathbf{U} converts the m weighted orthogonal inputs into the output column-vector ψ of size m . A meaningful comparison of $\bar{\mathbf{T}}$ with its counterpart based on a continuum model must be restricted to comparisons of the matrices \mathbf{S} and \mathbf{V} , as they control how the input is structured. In contrast, the matrix \mathbf{U} controls how the input is converted into the output in the domain of interest. Details of that conversion are significantly affected by the local microstructural details and therefore cannot be captured by the continuum model.

Now let us focus our attention to the transmission matrix corresponding to the simplest continuum model, governed by the Dirichlet boundary-value problem for Laplace's equation:

$$\nabla^2 u(\mathbf{x}) = 0 \quad \mathbf{x} \in \Omega \quad \text{and} \quad u(\mathbf{x}) = \phi(\mathbf{x}) \quad \mathbf{x} \in \partial\Omega. \quad (3.3)$$

Here we slightly abuse the notation by treating all quantities as continuous but keeping the symbols that have been used for discrete quantities. The transmission operator (infinite-dimensional matrix) for this problem follows

directly from Poisson's formula

$$\psi(\theta) = \mathcal{T}\phi(\theta) = \frac{1}{2\pi} \int_0^{2\pi} \frac{R^2 - r^2}{R^2 + r^2 - 2rR \cos(\theta - \theta')} \phi(\theta') d\theta'. \quad (3.4)$$

The spectral properties of this operator are well known since

$$\mathcal{T} \begin{pmatrix} \cos k\theta \\ \sin k\theta \end{pmatrix} = \left(\frac{r}{R}\right)^k \begin{pmatrix} \cos k\theta \\ \sin k\theta \end{pmatrix} \quad k = 0, 1, 2, \dots \quad (3.5)$$

The nontrivial eigen-pair corresponding to $k = 0$ represents rigid body motion.

A finite-dimensional analog of \mathcal{T} is obtained by (i) evaluating ψ at m uniformly spaced angular locations and (ii) replacing the integral with a Riemann's sum involving n terms. As a result we obtain

$$\mathbf{T} = \mathbf{USV}^*$$

with

$$U_{ij} = \sqrt{\frac{1}{m}} \begin{cases} 1 & \text{if } j = 1 \\ \sqrt{2} \cos \frac{\pi i j}{m} & \text{if } j \text{ is even} \\ \sqrt{2} \sin \frac{\pi i(j-1)}{m} & \text{if } j \text{ is odd and greater than 1} \end{cases} \quad (3.6)$$

$$S_i = \sqrt{\frac{m}{n}} \begin{cases} 1 & \text{if } i = 1 \\ \left(\frac{r}{R}\right)^{i/2} & \text{if } i \text{ is even} \\ \left(\frac{r}{R}\right)^{(i-1)/2} & \text{if } i \text{ is odd and greater than 1} \end{cases} \quad (3.7)$$

$$V_{ij} = \sqrt{\frac{1}{n}} \begin{cases} 1 & \text{if } j = 1 \\ \sqrt{2} \cos \frac{\pi i j}{n} & \text{if } j \text{ is even} \\ \sqrt{2} \sin \frac{\pi i(j-1)}{n} & \text{if } j \text{ is odd and greater than 1} \end{cases} \quad (3.8)$$

The indices run from 1 to m in (3.6) and (3.7) and from 1 to n in (3.8). Note that the matrices \mathbf{U} and \mathbf{V} are unitary only if m and n are odd numbers. For even numbers the matrices are no longer unitary but the columns remain orthogonal.

The trigonometric structure of the \mathbf{V} -matrix implies that the processed input $\mathbf{V}^*\boldsymbol{\phi}$ is a superposition of waves generated by the functions $\cos(k\theta)$ and $\sin(k\theta)$. Accordingly, one should expect that the continuum model may be useful only for $k < k_0$, where k_0 is a threshold wave number that depends on tolerance ϵ and possibly other problem parameters.

3.4 Simulation Results

In this section, we present simulation results that allow us to identify inputs $\boldsymbol{\phi}_0$ for which the outputs $\bar{\mathbf{T}}\boldsymbol{\phi}_0$ and $\mathbf{T}\boldsymbol{\phi}_0$ are sufficiently close. Furthermore, we establish that those inputs are identified by an ϵ -dependent minimum wave length λ_0 .

All computational results reported here were obtained using Monte-Carlo simulations traversing the space spanned by the parameters δ , Δ , and ρ as defined in Figure 3.1. For each point of that space we conducted 100 realizations. For each ten realizations, the nodal positions inside the circle of radius ρ were fixed, while the nodal positions inside the ring of thickness Δ were generated anew. We found that statistics generated in this manner was sufficiently accurate for our purposes. Moreover, it appears that our conclusions would not be affected if we conducted the entire study using only one lattice

realization inside the circle of radius ρ . The quantity of interest for Monte-Carlo simulations was the ensemble average $\bar{\mathbf{T}}(\delta, \Delta, \rho)$, and the corresponding \mathbf{S} and \mathbf{V} matrices.

To compare the transmission through lattices versus continuum we computed the difference between the corresponding singular values s_i versus s_i and column-vectors of \mathbf{V} versus \mathbf{V} . Both s_i and \mathbf{V} were computed as prescribed in (3.7) and (3.8). For the i -th singular values, the error was defined as

$$e_{s_i} = \left| \frac{s_i - s_i}{s_i} \right|. \quad (3.9)$$

For the i -th column-vectors the error was defined as

$$e_{v_i} = \sqrt{\sum_{j=1}^n (v_{ji} - v_{ji})^2}. \quad (3.10)$$

There is no need to normalize this error because both v_{ji} and v_{ji} are unit vectors.

In Figure 3.2, we show three plots for the error e_{v_i} versus the mode number i for three cases corresponding to

- (a) $\rho = 25, \delta = 5, \Delta = 5$
- (b) $\rho = 25, \delta = 5, \Delta = 15$
- (c) $\rho = 25, \delta = 5, \Delta = 25$.

These plots reveal that as Δ increases the curve e_{v_i} versus i approaches the shape characterized by a sharp transition. The transition occurs somewhere

between the 20th and 30th modes, and it signifies that the errors in the post-transition interval are very large. Before the transition, the errors are in the range between 10% and 30%. In this regard, let us mention that this level of errors is typical for simulations we performed.

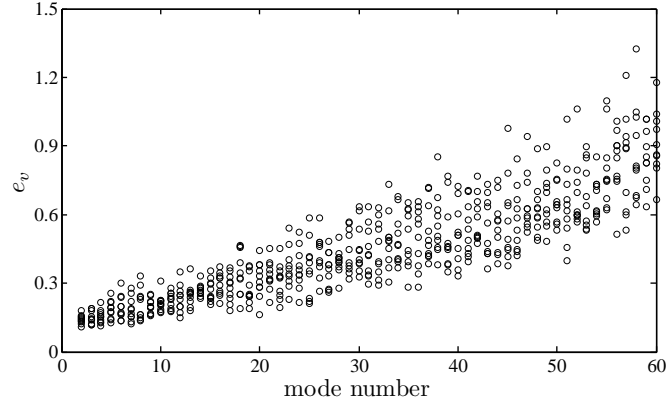
In Figure 3.3, we show five modes corresponding to $\rho = 25$, $\delta = 5$, and $\Delta = 20$. There the continuous lines and discrete symbols represent the exact and approximate solutions, respectively. These plots reaffirm the tendency revealed in Figure 3.2 – the quality of approximate solutions deteriorates for high order modes. Again, even for the first non-trivial mode $\cos \theta$ the error is above 10%.

In Figure 3.4, we show three plots for the error e_{v_i} versus the mode number i for three cases corresponding to e_{v_i} versus the mode number i for three cases corresponding to

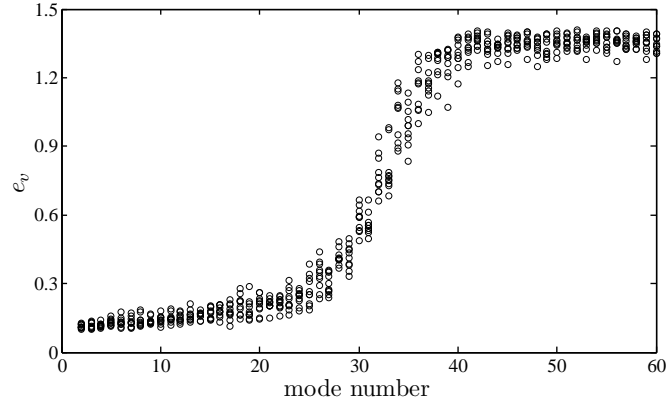
- (a) $\rho = 20$, $\delta = 2$, $\Delta = 20$
- (b) $\rho = 20$, $\delta = 5$, $\Delta = 20$
- (c) $\rho = 20$, $\delta = 10$, $\Delta = 20$.

These plots reveal that for a sufficiently large Δ the curve e_{v_i} versus i is rather insensitive to the value of δ as long as it exceeds several lattice spacings.

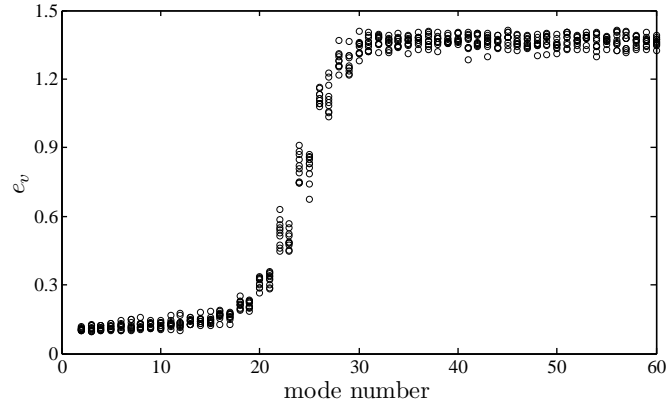
Based on simulation results presented in Figures 3.2 through 3.4, we would like to make the following proposition:



(a)



(b)



(c)

Figure 3.2: Error e_{v_i} versus the mode number i for (a) $\rho = 25$, $\delta = 5$, $\Delta = 5$; (b) $\rho = 25$, $\delta = 5$, $\Delta = 15$; (c) $\rho = 25$, $\delta = 5$, $\Delta = 25$.

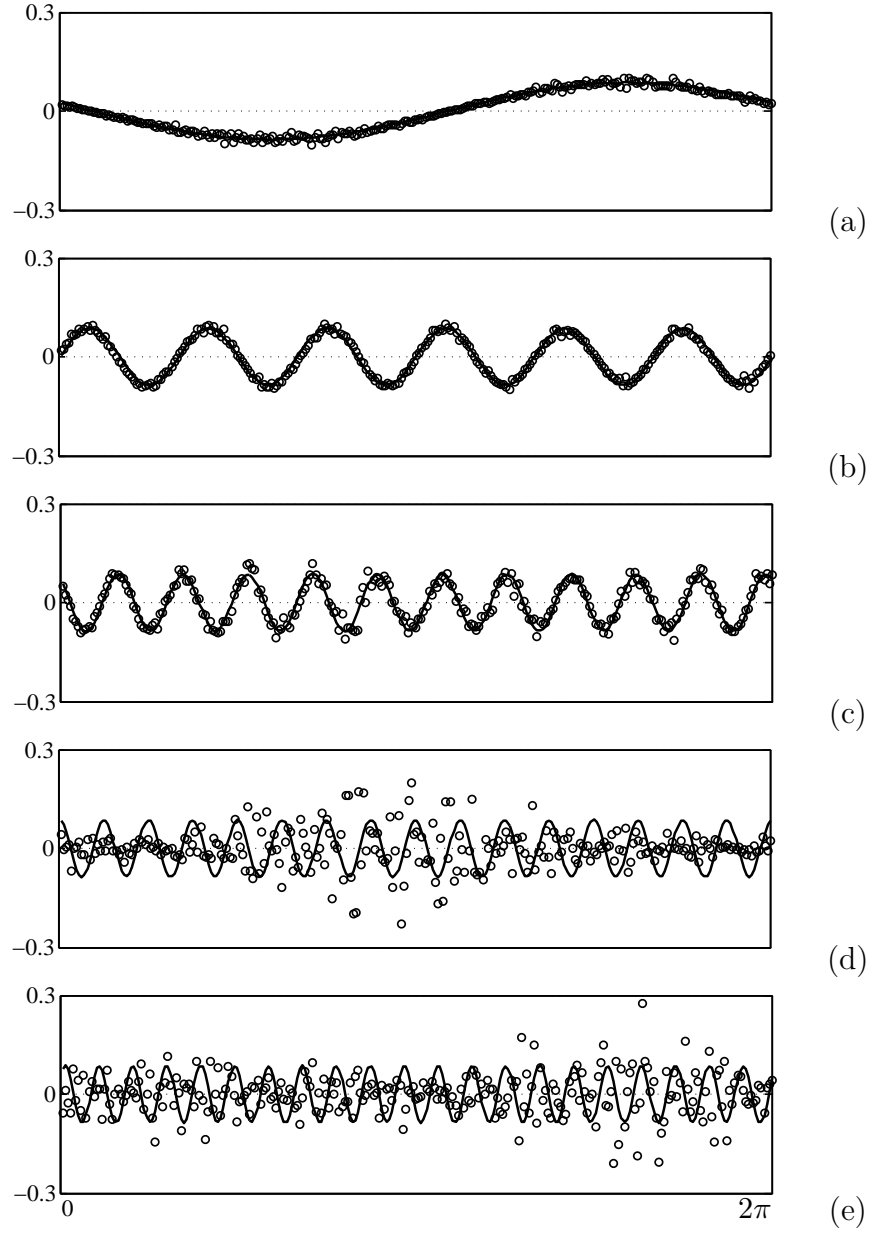
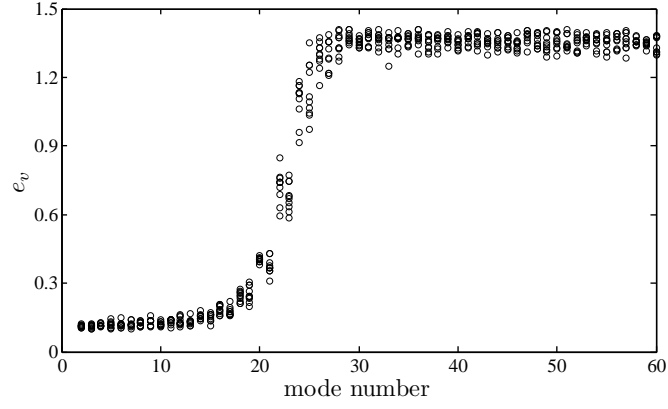
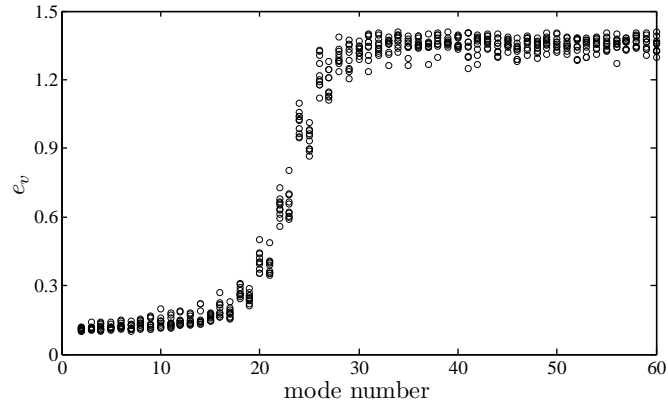


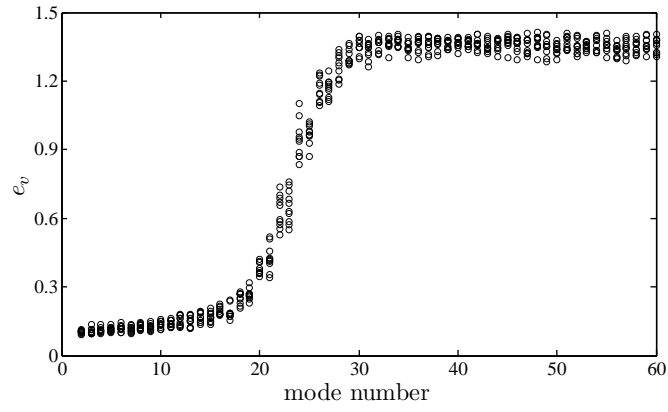
Figure 3.3: Discrete (symbols) versus continuum (lines) modes for $\rho = 25$, $\delta = 5$, $\Delta = 20$: (a) mode number 2 ($e_{v_2} = 0.11$), (b) mode number 12 ($e_{v_{12}} = 0.14$), (c) mode number 22 ($e_{v_{22}} = 0.27$), (d) mode number 32 ($e_{v_{32}} = 1.30$), (e) mode number 42 ($e_{v_{42}} = 1.34$). The threshold for $\epsilon = 0.3$ is $i_0 = 23$ and the wave number $k_0 = 11$.



(a)



(b)



(c)

Figure 3.4: Error e_{v_i} versus the mode number i for (a) $\rho = 20$, $\delta = 2$, $\Delta = 20$; (b) $\rho = 20$, $\delta = 5$, $\Delta = 20$; (c) $\rho = 20$, $\delta = 10$, $\Delta = 20$.

For a prescribed tolerance ϵ there exist δ_0 , Δ_0 , and $i_0(\rho)$ such that, for lattices with $\delta > \delta_0$ and $\Delta > \Delta_0$, $e_{v_i} < \epsilon$ for any $i < i_0(\rho)$. In less formal terms, this proposition implies that the continuum solutions are good approximations for adequately shielded domains of interest and sufficiently low modes. Our simulation results suggest that for $\epsilon = 0.3$, $\delta_0 = 2$ and $\Delta_0 = 10$.

Dependence of the threshold i_0 on ρ is unsettling because the threshold should be a lattice property. This issue is resolved by introducing the threshold wavelength

$$\lambda_0 = \frac{\pi\rho}{i_0} . \quad (3.11)$$

A plot λ_0 versus ρ supports the proposition that in the range between $10 \leq \rho \leq 25$ a constant $\lambda_0 \approx 13$ may be used as a uniquely defined threshold for $\epsilon = 0.3$ (Fig. 3.5). We repeated the entire study using e_{s_i} rather than e_{v_i} as the error indicator. This did not change the overall trend but led to a slightly lower threshold $\lambda_0 \approx 12$.

3.5 Closing Remarks

In this work, we attempted to determine the usefulness of continuum models for constructing approximate solutions for large lattices without actually specifying parameters of the continuum model. Instead we defined a restricted class of continuum models and determined conditions under which solutions of such models are sufficiently close to the exact solutions. This point of view departs from the RVE-centric approaches in which the principal

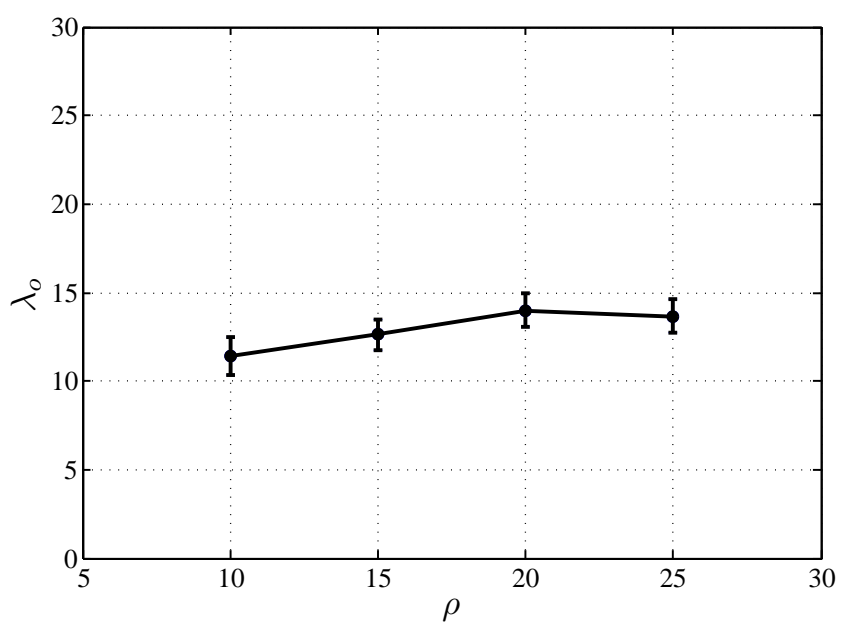


Figure 3.5: The threshold wavelength λ_0 versus ρ .

quantities of interest are tied directly to the RVE. Therefore it is interesting to compare these two points of view. Since each approach involves a macroscopic length scale, it is meaningful to compare the threshold wave length λ_0 , central to our approach, to the minimum RVE size l_0 , central to the conventional approach. For this purpose, we computed the coefficient of variation for the overall shear modulus, under prescribed linear displacements, as a function of the RVE diameter. The curve is shown in Figure 3.6. RVEs were generated by computing 100 realizations for each size. This curve implies that even for the smallest RVE's the coefficient of variation is well below the tolerance $\epsilon = 0.3$ we had to adopt for analyzing the transmission. Thus the conventional approach dramatically underestimates the minimum length scale at which solutions of the continuum model can be used for approximating solutions of the discrete model.

Our work can be regarded as a small step toward asking a much more general question: What would be an ϵ -dependent optimal (minimal) representation (model) of the lattice? Such representations are central to multiresolution analysis that includes wavelets, multigrid, and fast multipole methods. The essential ingredients of multi-resolution representations are hierarchy of coarse-scale models, data compression, and cross-scale data passing. Particulars of these ingredients are determined as part of the optimization procedure. This view of multiscale modeling has been already explored using wavelets [4, 30, 108] and multigrid [65, 87] methods. Connections between multiresolution methodology and multiscale modeling become transparent if one con-

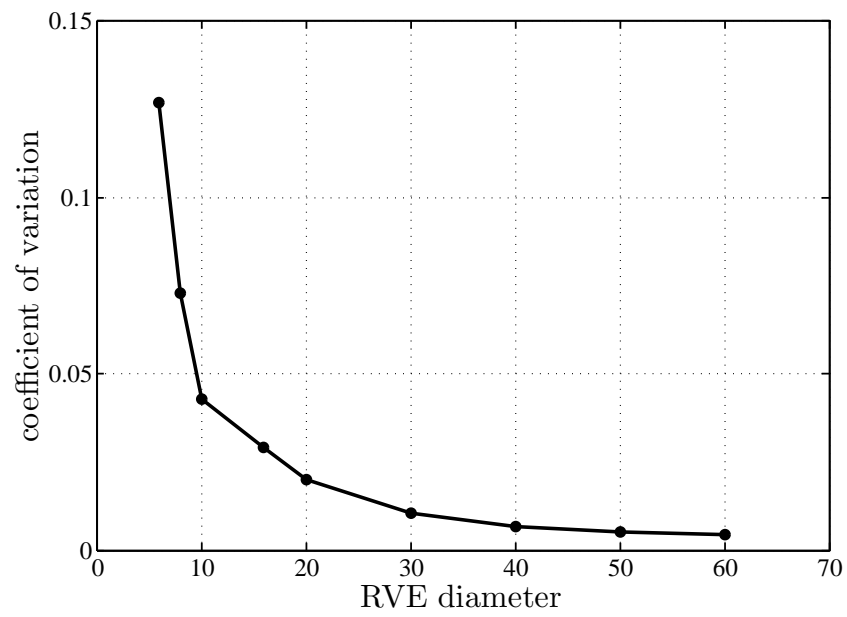


Figure 3.6: The coefficient of variation for the overall shear modulus versus the RVE diameter.

siders the fast multipole method [43] as an example. That method includes data compression (use of multipole and local moments), cross-level data passing (multipole-to-multipole and local-to-local translations), and a hierarchy of single-coarse-scale models (multipole-to-local translations). It is interesting to observe that the original version of the fast multipole method is based on spherical harmonics and has strong connections with classical electrostatics. In contrast, recent versions of the fast multipole method [41, 81] are based on linear algebraic tools, which optimize the performance but are difficult to relate to physical models. Let us also single out the so-called equation-free approach [61] in which the coarse-scale models are created on the fly by projecting the governing equations of the fine-scale model on coarse scales. This approach has been applied to a variety of interesting problems [11, 34, 60, 74] that involve non-linear dynamical systems. Those problems and consequently pertinent numerical methods are difficult to analyze, so that reliability of simulation results is a major issue.

Chapter 4

On Extension of Boundary Algebraic Equations to Irregular Lattices

4.1 Introduction

This chapter is motivated by Martinsson and Rodin's papers [79, 80] where they developed boundary algebraic equations (BAEs) for solving problems defined on regular lattices. BAEs share many features with boundary integral equations. The latter are related to linear partial differential equations, whereas the former are related to finite difference equations. Haq *et al.* [46] applied BAE to solving non-linear problems involving defects in regular infinite lattices. In that paper, the defect core, where non-linearities were important, was represented by finite difference equations, whereas a BAE was used for representing the surrounding linear lattice. As a result the original problem was reduced to a relatively small non-linear algebraic problem defined on the core. Thus this approach exploited the property that, like integral equations, BAEs are particularly effective for solving problems involving infinite domains.

In this chapter, we attempt to extend BAEs to irregular lattices. Such an extension would be indispensable for solving multiscale problems defined on

irregular lattices, as BAEs provide a seamless transition to remote boundary conditions. However, it is shown that, BAEs for irregular lattices contain certain terms may require the same amount of computational effort as the original problem for which the equations are formulated. In this chapter, we formulate a BAE for a model problem and expose the fundamental obstacle that prevents us from using that BAE as an effective tool. Nevertheless, the new BAE, and its extensions, may be treated within a statistical setting, which has not been explored in this work.

This chapter is structured as follows. In Section 4.2, we define a particular type of irregular lattices and define various lattice subdomains of interest. This restriction is not essential – all we need is a well defined process for constructing irregular lattices. In Section 4.3, we define Green’s function for a finite irregular lattices. In Section 4.4, we define model problems for finite and infinite and formulate the corresponding BAEs. In Section 4.5, we summarize the difficulties associated with those BAEs and outline possible avenues for future research.

4.2 Lattices

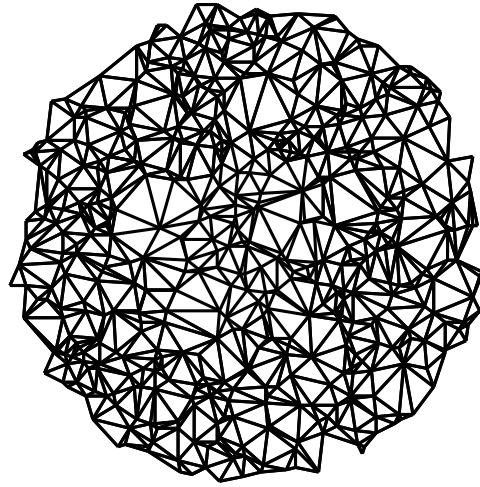
Consider a three-dimensional irregular lattice formed by tetrahedral cells. Mechanically, such a lattice behaves like a truss, so that the lattice bonds (truss bars) transmit axial forces only. Numerically, such lattices can be constructed using the following procedure: (i) generate nodes as a set of points whose cartesian coordinates are uniformly distributed random variables,

and (ii) use Delaunay triangulation to connect the nodes with the bonds.

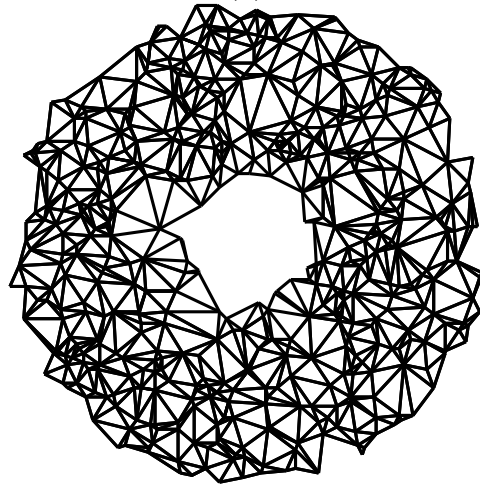
A quasi-spherical lattice domain is constructed by taking a large lattice and discarding all the nodes lying outside of a prescribed sphere and all the bonds connected to at least one node lying outside of the sphere. The exterior nodes of a lattice structure are defined as the set of vortices of the largest polyhedra whose edges are lattice bonds. We use the symbols Γ and Ω to denote the lattice nodes and subdomains, respectively. The exterior nodes of Ω are defined by $\partial\Omega$.

Let us consider two lattices. The first one is constructed as a quasi-spherical lattice of radius R ; we refer to this lattice as Ω (Figure 4.1a). The second lattice is formed by cutting out a concentric quasi-spherical void Ω^- from Ω . The void radius is denoted by r and the resulting spherical shell is denoted by Ω^+ (Figure 4.1b). Note that $\Gamma = \Gamma^+ \cup \Gamma^-$ but $\Omega \neq \Omega^+ \cup \Omega^-$, because the lattice $\Omega^+ \cup \Omega^-$ is disjoint as it does not include the bonds who have one node in Γ^+ and the other in Γ^- . We denote those bonds by Ω^0 . We define the exterior nodes of Ω^+ as the exterior nodes of Ω and denote them by Γ^e . We denote the interior boundary nodes of Ω^+ by Γ^i and define them as the set of nodes connected by the bonds Ω^0 to the nodes $\partial\Omega^-$ (Figure 4.1c). The assumption that the radii and the shell thickness are sufficiently larger in comparison to a typical bond length is implicit in all adopted definitions.

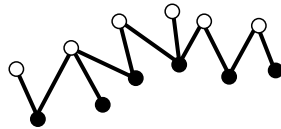
Infinite lattices are defined by considering sequences of finite lattices. For example, for quasi-spherical lattices, we consider a sequence constructed such that each lattice of radius R_n contains all the nodes of the lattice of ra-



(a)



(b)



(c)

Figure 4.1: (a) Quasi-spherical domain Ω ; (b) Quasi-spherical shell Ω^+ ; (c) The interface between Ω^- and Ω^+ involving the nodes $\partial\Omega^-$ (solid circles) and Γ^i (unfilled circles), and the bonds Ω^0 .

dius R_{n-1} and the remaining nodes are added with the same node density as the node density in R_{n-1} . Of course this sequence implies that $\Gamma_0 \subset \Gamma_1 \subset \Gamma_2 \dots \subset \Gamma_{n-1} \subset \Gamma_n$. It is clear that sequences constructed in this manner involve lattices that have to be treated as random variables. Thus we suppose that the lattice Ω_0 is prescribed and treat it as a deterministic entity; consequently quantities of interest associated with Ω_0 are treated deterministically. In contrast, for $n > 0$, quantities of interest associated with Ω_n , are treated as random variables. Similar sequences can be constructed for quasi-spherical shells Ω^+ .

4.3 Green's Function

Green's function \mathbf{U}_{ij} is defined via a map relating the displacement \mathbf{u}_i at a node i of Ω to a nodal force \mathbf{p} applied at a node j :

$$\mathbf{u}_i = \mathbf{U}_{ij} \cdot \mathbf{p} . \quad (4.1)$$

The displacements are defined with the provision that $\mathbf{u}_k = \mathbf{0}$ for all $k \in \partial\Omega$, and all nodes other than the node j and the exterior nodes are not loaded. Thus Green's function \mathbf{U}_{ij} is a square matrix whose entries are second rank tensors.

4.4 Boundary Algebraic Equation

In this section, we develop a BAE for a model problem defined for the shell Ω^+ subjected to an external linear constraint $\mathbf{u}_i = \boldsymbol{\epsilon}^0 \cdot \mathbf{x}_i$ for $i \in \Gamma^e$ and

not loaded at nodes other than Γ^e . Here $\boldsymbol{\epsilon}^0$ is a constant symmetric second-rank (strain) tensor. We denote the displacements and forces associated with this problem by \mathbf{u} and \mathbf{f} , respectively, and refer to these quantities as the main elastic state.

To construct the BAE we introduce an auxiliary elastic state of Ω^+ that involves Green's function defined on Ω . To this end, we first subject Ω to conditions involved in the definition of Green's function, so that the displacements are $\mathbf{U}_{ij} \cdot \mathbf{p}$. Next, we cut through the connecting bonds Ω^0 and thus cut Ω^+ out of Ω . To maintain the displacements $\mathbf{U}_{ij} \cdot \mathbf{p}$, we subject Ω^+ to the forces transmitted through the bonds Ω^0 to its interior boundary nodes Γ^i . Thus the auxiliary elastic state of Ω^+ is characterized by non-zero forces only on the nodes Γ^i and Γ^e ; we denote those forces by $\mathbf{F}_{ij} \cdot \mathbf{p}$.

The BAE is constructed by applying the Maxwell-Betty reciprocity theorem to the main and auxiliary elastic states of Ω^+ :

$$\mathbf{u}_j + \sum_{i \in \Gamma^i \cup \Gamma^e} \mathbf{F}_{ij} \cdot \mathbf{u}_i = \sum_{i \in \Gamma^i \cup \Gamma^e} \mathbf{U}_{ij} \cdot \mathbf{f}_i \quad j \in \Omega^+. \quad (4.2)$$

A more specific form of this equation is obtained by recognizing that $\mathbf{f}_i = \mathbf{0}$ for $i \in \Gamma^i$, $\mathbf{U}_{ij} = 0$ for $i \in \Gamma^e$, and $\mathbf{u}_i = \boldsymbol{\epsilon}^0 \cdot \mathbf{x}_i$ for $i \in \Gamma^e$:

$$\mathbf{u}_j + \sum_{i \in \Gamma^i} \mathbf{F}_{ij} \mathbf{u}_i = - \sum_{i \in \Gamma^e} \mathbf{F}_{ij} \cdot \boldsymbol{\epsilon}^0 \cdot \mathbf{x}_i \quad j \in \Gamma^i. \quad (4.3)$$

Here we restrict the nodes j to Γ^i as this is sufficient for solving for the unknown displacements.

BAE (4.3) must be modified if one is interested in solving problems for infinite lattices. This is necessary because the sum over Γ^e is not well defined for infinite lattices. To address this issue let us consider a BAE for Ω , rather than Ω^+ , subjected to an external linear constraint $\mathbf{u}_i = \boldsymbol{\epsilon}^0 \cdot \mathbf{x}_i$ for $i \in \Gamma^e$:

$$\mathbf{v}_j + \sum_{i \in \Gamma^e} \mathbf{F}_{ij} \cdot \mathbf{v}_i = \sum_{i \in \Gamma^e} \mathbf{U}_{ij} \cdot \mathbf{g}_i \quad j \in \Gamma^i. \quad (4.4)$$

Here \mathbf{v} and \mathbf{g} are the displacements and forces induced by the linear constraint imposed on Ω . The problem-specific form of (4.4) is

$$\mathbf{v}_j + \sum_{i \in \Gamma^e} \mathbf{F}_{ij} \cdot \boldsymbol{\epsilon}^0 \cdot \mathbf{x}_i = \mathbf{0} \quad j \in \Gamma^i. \quad (4.5)$$

Now we can combine (4.3) and (4.5) to obtain a BAE that does not involve summation over the nodes Γ^e :

$$\mathbf{u}_j + \sum_{i \in \Gamma^i} \mathbf{F}_{ij} \mathbf{u}_i = \mathbf{v}_j \quad j \in \Gamma^i. \quad (4.6)$$

In a deterministic setting, this BAE does not pose difficulties associated with extending the quasi-spherical spherical lattice to infinity. In particular, if the lattice were regular, then the tensor \mathbf{F}_{ij} could be constructed in a straightforward manner and the right-hand side is simply $\mathbf{v}_j = \boldsymbol{\epsilon}^0 \cdot \mathbf{x}_j$. In contrast, for irregular lattices, (4.6) requires a statistical treatment. Furthermore, for irregular lattices, the right-hand side \mathbf{v}_j is as difficult to construct as the solution of interest itself.

4.5 Summary

In this chapter, we developed a BAE relevant to analyzing defects in irregular lattices. Nevertheless, this BAE requires statistical treatment and its right-hand-side is as difficult to compute as the solution itself. In contrast, for regular lattices, the BAE can be treated deterministically and the right-hand-side is very easy to compute. Thus, for now, the idea of applying BAEs to irregular lattices is not attractive. An appropriate statistical setting for this problem is very challenging and is not pursued here.

Chapter 5

Concluding Remarks

In this dissertation, we presented three studies involving regular and irregular lattices. In the first study, concerned with characterization of near threshold behavior of subcritical cracks, the adopted regular lattice model was the simplest model that allowed us to demonstrate existence of the resistance T -curve. It would be exceedingly optimistic to expect from that model to provide any quantitative predictions but it was ideal for establishing a qualitative trend. In the second study, relationships between microscopic discrete and macroscopic continuum models were approached in a way that differs significantly from those well accepted in the research community. In particular, instead of focusing on the definition of the representative volume element, as it is usually done in the literature, we focused on how errors associated with the continuum model affect the microscopic quantities of interest. Furthermore, in contrast to the majority multiscale models involving continuum components, we engage the continuum model not as a component of a multiscale model, but rather as a generator of a limited approximation basis for exact solutions of boundary-value problems defined for the exact lattice model. Thus our approach is more in line with the current trend in multiscale modeling and computing, where it is necessary not only to determine macroscopic model pa-

rameters but also to control the quality of transmission of data passed from the macroscopic to microscopic scales. In the third study, an attempt was made to extend boundary algebraic equations, developed for regular lattices, to irregular lattices. Although resulting boundary algebraic equations are difficult to solve, it may be interesting to consider their treatment within an appropriate statistical setting. This is a very interesting direction for future research.

In closing, let us suggest that we expect that lattice-based modeling and computing will play a greater role in the future than it plays presently. Indeed, originally continuum models were introduced to suppress various microscopic, molecular, and atomistic scale effects. With the current trend in multiscale modeling and computing, where bridging of continuum and atomistic scales is often of primary concern, continuum models become somewhat of a liability, as they require very fine discretization and often give rise to singularities and other artificial undesired effects. Of course, continuum models are indispensable over large spatial (and temporal) scales, and the challenge is to identify hybrid models that combine the beneficial features of discrete and continuum models. Also, advances in nano-manufacturing are expected to lead to lattice-based optimal material designs for a variety of microelectronics, energy, and medical applications. Inevitably, those advances will spur the development of better lattice models.

Bibliography

- [1] F. F. Abraham and H. Gao. How fast can cracks propagate? *Phys. Rev. Lett.*, 84(14):3113–3116, 2000.
- [2] M. J. Alava, P.K.V.V. Nukala, and S. Zapperi. Statistical models of fracture. *Advances in Physics*, 55(3-4):349–476, May-June 2006.
- [3] M. P. Allen and D. J. Tildesley. *Computer simulation of liquids*. Oxford University Press, Oxford, 1989.
- [4] U. Andersson, B. Engquist, G. Ledfelt, and O. Runborg. A contribution to wavelet-based subgrid modeling. *Appl. Comput. Harmon. Anal.*, 7(2):151–164, 1999.
- [5] I. Babuška, R. Lipton, and M. Stuebner. The penetration function and its application to microscale problems. *BIT Numerical Mathematics*, 48(2):167–187, 2008.
- [6] I. Babuška and T. Strouboulis. *The finite element method and its reliability*. Oxford University Press,, 2001.
- [7] Z. P. Bazant, M. R. Tabbara, M. T. Kazemi, and G. Pijaudier-Cabot. Random particle model for fracture of aggregate or fiber composites. *Journal of Engineering Mechanics*, 116:1686–1705, 1990.

- [8] P. D. Beale and D. J. Srolovitz. Elastic fracture in random materials. *Phys. Rev. B*, 37:5500–5507, 1988.
- [9] G. I. Bell. Models for specific adhesion of cells to cells. *Science*, 200:618–627, 1978.
- [10] A. Bensoussan, J.-L. Lions, and G. Papanicolaou. *Asymptotic analysis for periodic structures*. North-Holland Publishing Co., Amsterdam, 1978.
- [11] A. Bindal, M. G. Ierapetritou, S. Balakrishnan, A. Armaou, A. G. Makeev, and I. G. Kevrekidis. Equation-free, coarse-grained computational optimization using timesteppers. *Chemical Engineering Science*, 61(2):779–793, 2006.
- [12] D. Bonamy. Intermittency and roughening in the failure of brittle heterogeneous materials. *Journal of Physics D – Applied Physics*, 42(21):214014, November 2009.
- [13] M. Born. Zur raumgittertheorie des diamanten. *Annalen der Physik*, 44:605–642, 1914.
- [14] M. Born and K. Huang. *Dynamical theory of crystal lattices*. Oxford University Press, New York, 1954.
- [15] M. Born and T. von Kármán. Über schwingungen in raumgittern. *Phys. Z.*, 13:297–309, 1912.

- [16] D. Broek. *Elementary engineering fracture mechanics*. Kluwer Academic Publishers Group, 1982.
- [17] M. J. Buehler. *Atomistic modeling of materials failure*. Springer, 2008.
- [18] N. J. Burt and J. W. Dougill. Progressive failure in a model heterogeneous medium. *J. Engrg. Mech. Div., ASCE*, 103(3):365–376, 1977.
- [19] E. D. Case, J. R. Smyth, and J. R. O. Hunter. Microcrack healing during the temperature cycling of single phase ceramics. In *Fracture Mechanics of Ceramics, Vol. 5*, pages 507–530. Plenum Press, New York, 1983.
- [20] K. S. Chan and R. A. Page. Origin of the creep-crack growth threshold in a glass-ceramic. *Journal of the American Ceramic Society*, 75:603–612, 1992.
- [21] Y. Charles, D. Vandembroucq, F. Hild, and S. Roux. Material-independent crack arrest statistics. *Journal of the Mechanics and Physics of Solids*, 52(7):1651–1669, July 2004.
- [22] J. C. Charmet, S. Roux, and E. Guyon, editors. *Disorder and fracture*. Plenum Press, New York, 1990.
- [23] W. Chen and J. Fish. A generalized space-time mathematical homogenization theory for bridging atomistic and continuum scales. *Int. J. Numer. Meth. Engng*, 67:253–271, 2006.

- [24] D. Cioranescu and J. Saint Jean Paulin. *Homogenization of reticulated structures*. Springer-Verlag, New York, 1999.
- [25] R. F. Cook. Environmentally-controlled non-equilibrium crack propagation in ceramics. *Materials Science and Engineering A*, 260:29–40, 1999.
- [26] R. M. Davis. *Space structures: A study of methods and developments in three-dimensional construction resulting from the international conference on space structures*. Wiley, New York, 1966.
- [27] A. R. Day, K. A. Snyder, E. J. Garboczi, and M. F. Thorpe. The elastic moduli of a sheet containing circular holes. *J. Mech. Phys. Solids*, 40:1031–1051, 1992.
- [28] V. S. Deshpande, N. A. Fleck, and M. F. Ashby. Effective properties of the octet truss material. Technical report, Cambridge university engineering department, 2000.
- [29] V. S. Deshpande, N. A. Fleck, and M. F. Ashby. Effective properties of the octet-truss lattice material. *Journal of the Mechanics and Physics of Solids*, 49:1747–1769, 2001.
- [30] M. Dorobantu and B. Engquist. Wavelet-based numerical homogenization. *SIAM J. Numer. Anal.*, 35(2):540–559 (electronic), 1998.

- [31] P. M. Duxbury, P. D. Beale, and P. L. Leath. Size effects of electrical breakdown in quenched random media. *Phys. Rev. Lett.*, 57:1052–1055, 1986.
- [32] W. E and B. Engquist. The heterogeneous multi-scale methods. *Comm. Math. Sci.*, 1:87–132, 2002.
- [33] K. Eom, D. M. Makarov, and G. J. Rodin. Theoretical studies of the kinetics of mechanical unfolding of cross-linked polymer chains and their implications for single-molecule pulling experiments. *Physical Review E*, 71(021904), 2005.
- [34] R. Erban, I. G. Kevrekidis, and H. G. Othmer. An equation-free computational approach for extracting population-level behavior from individual-based models of biological dispersal. *Physica D: Nonlinear Phenomena*, 215(1):1–24, 2006.
- [35] A. G. Evans and E. A. Charles. Strength recovery by diffusive crack healing. *Acta Metallurgica*, 25:919–927, 1977.
- [36] A. G. Evans, J. W. Hutchinson, and M. F. Ashby. Multifunctionality of cellular metal systems. *Progress in Materials Science*, 43(3):171–221, 1998.
- [37] M. W. Finnis and J. E. Sinclair. A simple empirical n -body potential for transition metals. *Phil. Mag. A*, 50:45–55, 1984.

- [38] J. Fish and C. Schwob. Towards constitutive model based on atomistics. *Journal of Multiscale Computational Engineering*, 1:43–56, 2003.
- [39] R. B. Fuller and E. J. Applewhite. *Synergetics: Exploration in the geometry of thinking*. McMillan Publishing Co., 1975.
- [40] L. J. Gibson and M. F. Ashby. *Cellular solids, structure and properties*. Pergamon Press, Exeter, 1989.
- [41] Z. Gimbutas and V. Rokhlin. A generalized fast multipole method for nonoscillatory kernels. *SIAM Journal on Scientific Computing*, 24(3):796–817, 2002.
- [42] M. Grah, K. Alzebdeh, P. Y. Sheng, M. D. Vaudin, K. J. Bowman, and M. Ostoj-Starzewski. Brittle intergranular failure in 2D microstructures: Experiments and computer simulations. *Acta Mater.*, 44(10):4003–4018, 1996.
- [43] L. Greengard and V. Rokhlin. A fast algorithm for particle simulations. *J. Comput. Phys.*, 73(2):325–348, 1987.
- [44] T. K. Gupta. Crack healing in thermally shocked MgO. *Journal of the American Ceramic Society*, 58(3–4):143–143, 1975.
- [45] S. Haq, A. B. Movchan, and G. J. Rodin. Analysis of lattices with non-linear interphases. *Acta Mechanica Sinica*, 22(4):323 – 330, 2006.

- [46] S. Haq, A. B. Movchan, and G. J. Rodin. Lattice Greens functions in nonlinear analysis of defects. *Journal of Applied Mechanics-Transactions of the ASME*, 74(4):686–690, 2007.
- [47] Z. Hashin. Analysis of composite materials - a survey. *Journal of Applied Mechanics*, 50:481–505, 1983.
- [48] G. N. Hassold and D. J. Srolovitz. Brittle fracture in materials with random defects. *Phys. Rev. B*, 39(13):9273–9281, 1989.
- [49] A. M. Hayes, A. Wang, B. M. Dempsey, and D. L. McDowell. Mechanics of linear cellular alloys. *Mechanics of Materials*, 36:691–713, 2004.
- [50] H. J. Herrman and S. Roux, editors. *Statistical models for the fracture of disordered media*. North-Holland, New York, 1990.
- [51] H. J. Herrmann, A. Hansen, and S. Roux. Fracture of disordered, elastic lattices in two dimensions. *Physical Review B*, 39(1):637–648, 1989.
- [52] A. Hrennikoff. Solution of problems of elasticity by the frame-work method. *ASME J. Appl. Mech.*, 8:A619–A715, 1941.
- [53] K. W. Jacobsen, J. K. Nørskov, and M. J. Puska. Interatomic interactions in the effective medium theory. *Phys. Rev. B*, 35(14):7423–7442, 1987.
- [54] S. Jacobsen, J. Marchan, and L. Boisvert. Effect of cracking and healing on chloride transport in OPC concrete. *Cement and Concrete Research*, 26(6):869–881, 1996.

- [55] W. Y. Jang. *On the compressive response of open-cell aluminum foams*. PhD thesis, University of Texas at Austin, 2010.
- [56] M. Jirasek and Z. P. Bazant. Macroscopic fracture characteristics of random particle systems. *International Journal of Fracture*, 69:201–228, 1995.
- [57] K. Jud and H. H. Kausch. Load transfer through chain molecules after interpenetration at interfaces. *Polymer Bulletin*, 1:697–707, 1979.
- [58] K. Jud, H. H. Kausch, and J. G. Williams. Fracture mechanics studies of crack healing and welding of polymers. *Journal of Materials Science*, 16:204–210, 1981.
- [59] P. N. Keating. Effect of invariance requirements on the elastic strain energy of crystals, with application to the diamond structure. *Phys. Rev.*, 145(2):637–645, 1966.
- [60] I. G. Kevrekidis, C. W. Gear, and G. Hummer. Equation-free: The computer-aided analysis of complex multiscale systems. *AIChE Journal*, 50(7):1346C1355, 2004.
- [61] I. G. Kevrekidis, C.W. Gear, J. M. Hyman, P. G. Kevrekidis, O. Runborg, and C. Theodoropolos. Equation-free, coarse-grained multiscale computation: Enabling microscopic simulators to perform system-level tasks. *Communications in Mathematical Sciences*, 1(4), 2003.

- [62] T. Kim, C. Y. Zhao, T. J. Lu, and H. P. Hodson. Convective heat dissipation with lattice-frame materials. *Mechanics of Materials*, 36:767–780, 2004.
- [63] J. G. Kirkwood. The skeletal modes of vibration of long chain molecules. *J. Chem. Phys.*, 7:506–509, 1939.
- [64] C. Kittel. *Introduction to solid state physics*. Wiley, New York, 1956.
- [65] S. Knappek. Matrix-dependent multigrid homogeneization for diffusion problems. *SIAM J. Sci. Comput.*, 20(2):515–533 (electronic), 1999.
- [66] R. Komanduri, N. Chandrasekaran, and L. M. Raff. Molecular dynamics (MD) simulations of uniaxial tension of some single-crystal cubic metals at nanolevel. *Int. J. Mech. Sci.*, 43:2237–2260, 2001.
- [67] R. Lakes. Negative Poisson’s ratio materials. *Science*, 235:1038–1040, 1987.
- [68] F. F. Lange and T. K. Gupta. Crack healing by heat treatment. *Journal of the American Ceramic Society*, 53(1):54–55, 1970.
- [69] B. R. Lawn. *Fracture of brittle solids*. Cambridge University Press, 1993.
- [70] S. Lee, F. Barthelat, J. W. Hutchinson, and H. D. Espinosa. Dynamic failure of metallic pyramidal truss core materials-experiments and modeling. *Int. J. Plasticity*, 22:2118–2145, 2006.

- [71] J. E. Lennard-Jones. On the determination of molecular fields. *Proc. R. Soc. Lond. A*, 106:463–477, 1924.
- [72] W. K. Liu, E. G. Karpov, and H. S. Park. *Nano mechanics and materials: Theory, multiscale methods and applications*. Wiley, 2006.
- [73] D. M. Makarov, P. K. Hansma, and H. Metiu. Kinetic Monte-Carlo simulation of titin unfolding. *Journal of Chemical Physics*, 114:9663–9673, 2001.
- [74] A. G. Makeev and I. G. Kevrekidis. Coarse-graining the computations of surface reactions: Nonlinear dynamics from atomistic simulators. *Surface Science*, 603:1696–1705, 2009.
- [75] A. A. Maradudin, E. W. Montroll, G. H. Weiss, Robert Herman, and H. W. Milnes. Green’s functions for monatomic simple cubic lattices. *Acad. Roy. Belg. Cl. Sci. Mém. Coll. in-4 deg. (2)*, 14(7):176, 1960.
- [76] P. G. Martinsson. *Fast multiscale methods for lattice equations*. PhD thesis, University of Texas at Austin, Computational and Applied Mathematics, 2002.
- [77] P. G. Martinsson and I. Babuška. Homogenization of materials with periodic truss or frame micro-structures. *Mathematical Models and Methods in Applied Sciences*, 17(5):805–832, 2007.
- [78] P. G. Martinsson and G. J. Rodin. Asymptotic expansions of lattice Green’s functions. *Proc. Royal Soc. A*, 458:2609 – 2622, 2002.

- [79] P. G. Martinsson and G. J. Rodin. Boundary algebraic equations for lattice problems. In *Proceedings of the IUTAM symposium on asymptotics, singularities and homogenization in problems of mechanics*. Kluwer, 2002.
- [80] P. G. Martinsson and G. J. Rodin. Boundary algebraic equations for lattice problems. *Proceedings of the Royal Society A*, 465:2489–2503, 2009.
- [81] P. G. Martinsson and V. Rokhlin. An accelerated kernel-independent fast multipole method in one dimension. *SIAM Journal on Scientific Computing*, 29(3):1160–1178, 2007.
- [82] R. Marx, F. Jungwirth, and P-O. Walter. Threshold intensity factors as lower boundaries for crack propagation in ceramics. *BioMedical Engineering OnLine*, 3:41, 2004.
- [83] D. McHenry. A lattice analogy for the solution of plane stress problems. *J. Inst. Civ. Eng.*, 21:59–82, 1943.
- [84] H. Metiu, Y. T. Lu, and Z. Y. Zhang. Epitaxial-growth and the art of computer-simulations. *Science*, 255:1088–1092, 1992.
- [85] Y. Mishin, M. J. Mehl, D. A. Papaconstantopoulos, A. F. Voter, and J. D. Kress. Structural stability and lattice defects in copper: Ab-initio, tight-binding and embedded-atom calculations. *Phys. Rev. B*, 63(224106), 2001.

- [86] P. M. Morse. Diatomic molecules according to the wave mechanics. ii. vibrational levels. *Phys. Rev.*, 34:57–64, 1929.
- [87] D. J. Moulton, J. E. Dendy, and J. M. Hyman. The black box multigrid numerical homogenization algorithm. *J. Comp. Phys.*, 142(1):80–108, 1998.
- [88] A. K. Noor. Continuum modeling for repetitive lattice structures. *Applied Mechanics Review*, 41(7):285–296, 1988.
- [89] M. Ostoja-Starzewski. Microstructural disorder, mesoscale finite elements and macroscopic response. *Proc. R. Soc. Lond. A*, 455:3189–3199, 1999.
- [90] M. Ostoja-Starzewski. Lattice models in micromechanics. *Appl. Mech. Rev.*, 55(1):35–60, 2002.
- [91] M. Ostoja-Starzewski, P. Y. Sheng, and K. Alzebdeh. Spring network models in elasticity and fracture of composites and polycrystals. *Computational Materials Science*, 7:82–93, 1996.
- [92] M. Ostoja-Starzewski, P. Y. Sheng, and I. Jasiuk. Influence of random geometry on effective properties and damage formation in composite materials. *ASME J. Engng Mater. Tech.*, 116:384–391, 1994.
- [93] M. Ostoja-Starzewski, P. Y. Sheng, and I. Jasiuk. Damage patterns and constitutive response of random matrix-inclusion composites. *Engineering Fracture Mechanics*, 58:581–606, 1997.

- [94] M. Ostoja-Starzewski and C. Wang. Linear elasticity of planar Delaunay networks: Random field characterization of effective moduli. *ACTA Mechanica*, 80:61–80, 1989.
- [95] M. Ostoja-Starzewski and X. Wang. Stochastic finite elements as a bridge between random material microstructure and global response. *Computational Methods in Applied Mechanics and Engineering*, 168:35–49, 1999.
- [96] D. Qian, G. J. Wagner, and W. K. Liu. A multiscale projection method for the analysis of carbon nanotubes. *Comput. Methods Appl. Mech. Eng.*, 193:1603–1632, 2004.
- [97] A. Rahman. Correlations in the motions of atoms in liquid Argon. *Phys. Rev.*, 136:A405–A411, 1964.
- [98] J. R. Rice. Thermodynamics of quasi-static growth of Griffith cracks. *Journal of the Mechanics and Physics of Solids*, 26(2):61–78, 1978.
- [99] R. E. Rudd and J. Q. Broughton. Concurrent coupling of length scales in solid state systems. *Phys. Status Solidi b*, 217:251–291, 2000.
- [100] C. Saltzer. Discrete potential theory for two-dimensional Laplace and Poisson difference equations. Technical Report 4086, National Advisory Committee on Aeronautics, 1958.
- [101] R. A. Schapery. On the mechanics of crack closing and bonding in linear viscoelastic media. *International Journal of Fracture*, 39:163–189, 1989.

- [102] E. Schlangen and E. J. Garboczi. New method for simulating fracture using an elastically uniform random geometry lattice. *Int. J. Engng. Sci.*, 34(10):1131–1144, 1996.
- [103] N. Shestopalov. Controlled self-assembly of charged monolayers. personal communication.
- [104] S. Shu, Y. Xiao, J. Xu, and L. Zikatanov. Algebraic multigrid methods for lattice block materials. In T. Chan, Y. Huang, T. Tang, J. Xu, and L.-A. Ying, editors, *Recent Progress In Computational And Applied PDEs*, pages 289–307, 2001.
- [105] O. Sigmund and S. Torquato. Design of materials with extreme thermal expansion using a three-phase topology optimization method. *J. Mech. Phys. Solids*, 45:1037–1067, 1997.
- [106] D. L. Smith and B. Evans. Diffusional crack healing in quartz. *Journal of Geophysical Research*, 89(B6):4125–4135, 1984.
- [107] K. A. Snyder, E. J. Garboczi, and A. R. Day. The elastic moduli of random twodimensional composites: Computer simulation and effective medium theory. *J. Appl. Phys.*, 72:5948–5955, 1992.
- [108] B. Z. Steinberg, J. J. McCoy, and M. Mirotznik. A multiresolution approach to homogenization and effective modal analysis of complex boundary value problems. *SIAM J. Appl. Math.*, 60(3):939–966, 2000.

- [109] G. Strang. *Introduction to applied mathematics*. Wellesley-Cambridge Press, 1986.
- [110] E. B. Tadmor, M. Ortiz, and R. Phillips. Quasicontinuum analysis of defects in crystals. *Phil. Mag. A*, 73:1529–1563, 1996.
- [111] E. B. Tadmor, G. S. Smith, N. Bernstein, and E. Kaxiras. Mixed finite element and atomistic formulation for complex crystals. *Physical Review B*, 59(1):235–245, 1999.
- [112] M. Thompson and M. Renauld. Evaluation of structural porous metals. Technical report, United Technologies - Research Center, 1997.
- [113] S. P. Timoshenko. *History of strength of materials*. McGraw-Hill, New York, 1953.
- [114] S. Torquato. *Random heterogeneous materials: microstructure and macroscopic properties*. Springer-Verlag, 2002.
- [115] F. Tzschichholz, H. J. Herrmann, H. E. Roman, and M. Pfuff. Beam model for hydraulic fracturing. *Phys. Rev. B*, 49:7056–7059, 1994.
- [116] M. Vogelius. A homogenization result for planar, polygonal networks. *RAIRO Modél. Math. Anal. Numér.*, 25(4):483–514, 1991.
- [117] A. F. Voter. Classically exact overlayer dynamics - diffusion of rhodium clusters on Rh(100). *Physical Review B*, 34:6819–6829, 1986.

- [118] G. J. Wagner and W. K. Liu. Coupling of atomistic and continuum simulations using a bridging scale decomposition. *J. Comput. Phys.*, 190:249–274, 2003.
- [119] J. C. Wallach and L. J. Gibson. Mechanical behaviour of three-dimensional truss structures. Technical report, Department of Materials Science and Engineering, MIT, 2000.
- [120] K. T. Wan, N. Aimard, S. Lathabai, R. G. Horn, and B. R. Lawn. Interfacial energy-states of moisture-exposed cracks in mica. *Journal of Materials Research*, 5(1):172–182, 1990.
- [121] K. T. Wan and B. R. Lawn. Surface forces at crack interfaces in mica in the presence of capillary condensation. *Acta Metallurgica et Materialia*, 38(11):2073–2083, 1990.
- [122] N. Wicks and J. W. Hutchinson. Optimal truss plates. Technical report, Div. of Eng. and Appl. Science, Harvard University, 2000.
- [123] S. M. Wiederhorn and P. R. Townsend. Crack healing in glass. *Journal of the American Ceramic Society*, 53(9):486–489, 1970.
- [124] R. P. Wool and K. M. O’Connor. A theory of crack healing in polymers. *Journal of Applied Physics*, 52(10):5953–5963, 1981.
- [125] S. P. Xiao and T. Belytschko. A bridging domain method for coupling continua with molecular dynamics. *Comput. Methods Appl. Mech. Eng.*, 193:1645–1669, 2004.

- [126] Y. Yokoo, T. Nakamura, K. Heki, and S. Kawamata. IASS tension structures and space frames. Technical report, Architectural Institute of Japan, Tokyo, Japan, 1971.
- [127] Z. Y. Zhang, K. Haug, and H. Metiu. Exact classical simulation of hydrogen migration on Ni(100) - the role of fluctuations, recrossing, and multiple jumps. *Journal of Chemical Physics*, 93:3614–3634, 1990.
- [128] H. F. Zhao, D. E. Makarov, and G. J. Rodin. The resistance curve for subcritical cracks near the threshold. *International Journal of Fracture*, 2010.
- [129] A. Zubelewicz and Z.P. Bazant. Interface element modelling of fracture in aggregate composites. *ASCE J. Engng Mech.*, 113:1619–1630, 1987.

Vita

Haifeng Zhao received a Bachelor of Engineering degree in July, 2002 from the Beijing Institute of Technology. As an honors student, he was awarded admission to the graduate school in Beijing Institute of Technology and received a Master of Science degree in December, 2004.

In January, 2005, he entered the University of Texas at Austin to pursue a Ph.D. degree in the Department of Aerospace Engineering and Engineering Mechanics, under the supervision of Dr. Gregory J. Rodin.

Permanent address: 2501 Lake Austin Blvd Apt F205
Austin, Texas, 78703

This dissertation was typeset with L^AT_EX[†] by the author.

[†]L^AT_EX is a document preparation system developed by Leslie Lamport as a special version of Donald Knuth's T_EX Program.